# TRIUMF

# ANNUAL REPORT
# SCIENTIFIC ACTIVITIES
# 2000

ISSN 1492-417X

**CANADA'S NATIONAL LABORATORY**
**FOR PARTICLE AND NUCLEAR PHYSICS**

OPERATED AS A JOINT VENTURE

MEMBERS:

THE UNIVERSITY OF ALBERTA
THE UNIVERSITY OF BRITISH COLUMBIA
CARLETON UNIVERSITY
SIMON FRASER UNIVERSITY
THE UNIVERSITY OF VICTORIA

ASSOCIATE MEMBERS:

THE UNIVERSITY OF MANITOBA
L'UNIVERSITÉ DE MONTRÉAL
QUEEN'S UNIVERSITY
THE UNIVERSITY OF REGINA
THE UNIVERSITY OF TORONTO

UNDER A CONTRIBUTION FROM THE
NATIONAL RESEARCH COUNCIL OF CANADA

OCTOBER 2001

*The contributions on individual experiments in this report are outlines intended to demonstrate the extent of scientific activity at TRIUMF during the past year. The outlines are not publications and often contain preliminary results not intended, or not yet ready, for publication. Material from these reports should not be reproduced or quoted without permission from the authors.*

## Experiment 704
## Charge symmetry breaking in $np \to d\pi^0$ close to threshold

*(A.K. Opper, Ohio; E. Korkmaz, UNBC)*

Experiment 704 expects to have a high precision measurement of charge symmetry breaking in the strong interaction completed by mid-2001. The observable of interest is the forward-backward asymmetry ($A_{fb}$) in $np \to d\pi^0$, which must be zero in the centre of mass if charge symmetry is conserved and has a predicted value that ranges between $(-35 \to +70) \times 10^{-4}$ [Niskanen, Few-Body Systems **26**, 241 (1999); van Kolck *et al.*, Phys. Lett. **B493**, 65 (2000)] depending on the strengths of the various contributions (see Fig. 35). The forward-backward asymmetry is defined as $A_{fb}(\theta) \equiv \frac{\sigma(\theta)-\sigma(\pi-\theta)}{\sigma(\theta)+\sigma(\pi-\theta)}$ with the relevant contributions being the neutron-proton mass difference ($\delta$), exchange of an isospin mixed $\eta-\pi$ meson, and the effect of the $d$ $u$ quark mass difference on pion nucleon scattering.

The experiment was carried out with a 279.5 MeV neutron beam, a liquid hydrogen target, and the SASP spectrometer positioned at 0°. With these kinematics and the large acceptance of SASP the full deuteron distribution was detected in one setting of the spectrometer, thereby eliminating many systematic uncertainties. Measurements of $np$ elastic scattering with incident neutron beams that fill the same target space and produce protons that span the momentum distribution of the $np \to d\pi^0$ reaction provide a stringent test of the acceptance description of the spectrometer. A measurement of the $pp \to d\pi^+$ distribution accompanied the primary measurement as a test of the analysis and simulation codes, since the deuteron distribution from $pp \to d\pi^+$ must be symmetric in the centre of mass. With over seven (ten) million $np \to d\pi^0$ ($pp \to d\pi^+$) events and six million $np$ elastic events, the statistical uncertainty of this measurement is $5 \times 10^{-4}$. The anticipated systematic uncertainty is $10 \times 10^{-4}$.

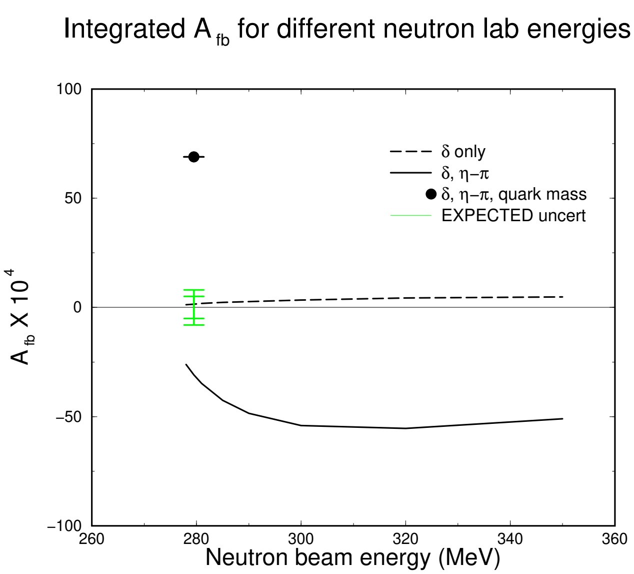


Fig. 35. Calculated contributions to $A_{fb}$ and *anticipated* uncertainties.

### Data analysis

Experiment 704 production data are analyzed in four successive passes: (1) detector calibration, (2) beam direction determination in the SASP-centric front end wire chamber coordinate system, (3) final extraction of the deuteron kinematic locus, and (4) efficiency determination. Analysis of all $np \to d\pi^0$ data had been completed by the end of 1999 and the $pp \to d\pi^+$ data analysis was completed a few months later.

Analysis efforts at the beginning of 2000 focused on developing and using code to determine the proton contamination and detection efficiencies for pions and protons in the $pp \to d\pi^+$ data as these are required in the simulation of this reaction. Thorough examination of these data uncovered anomalous wire hits which could not be correlated with problems in the FASTBUS readout system. Eventually an inconsistency between the readout code and the analysis code was discovered that led to the unusual hit patterns. The analysis code has since been modified to check for consistency between it and the readout code and make corrections if necessary. The first pass of the data to calibrate the detectors only uses events with a single cluster of wires in each of the front end wire chamber (FEC) planes. Consequently, events in which the additional hits led to multi-clusters in the wire planes were not used to calibrate the detectors and the effect of the code inconsistency was a small reduction in the statistical determination of the calibrations. A similar situation exists in the second pass of the analysis which determines the incident beam angle to within ± 0.10 mrad and showed a difference between 0.10 and 0.20 mrad when the new code was used. Although the effect of this on $A_{fb}$ was later shown to be small, all $np \to d\pi^0$ data were reanalyzed through the second pass and a combined third-fourth pass.

In addition to extracting the kinematic locus and detector efficiencies, the last pass of analysis also produced a filtered data set of 8 words/event (four target variables and four focal plane variables) for all good locus events. The filtered data set of ∼200 Mb can be re-sorted and analyzed in one hour on a Linux box. The

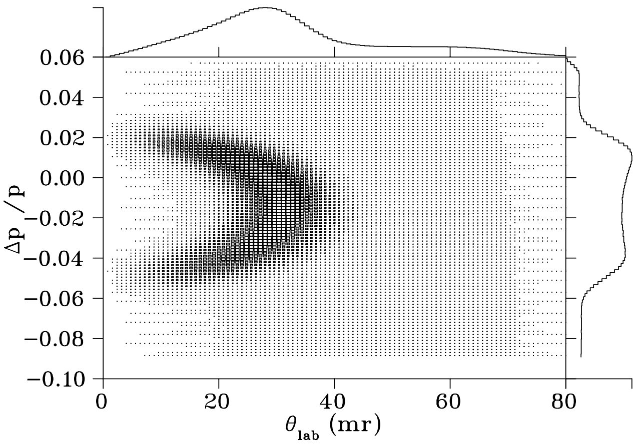


Fig. 36. Kinematic locus of all $np \rightarrow d\pi^0$ data.

reanalysis of the $np \rightarrow d\pi^0$ data took approximately two months and was finished at the end of September. The kinematic locus for these data is seen in Fig. 36. Three cycles of $pp \rightarrow d\pi^+$ data (November, 1997; July, 1997; August, 2000) have been reanalyzed and were used in the development of a $pp \rightarrow d\pi^+$ simulation. The reanalysis of the remaining $pp \rightarrow d\pi^+$ data is ongoing.

**GEANT simulation of Expt. 704**

At the beginning of the year a full review of the GEANT description of the experimental equipment was undertaken to verify consistency between it and reality. This description includes modelling of the beam, definition of all volumes and surfaces from the target to the focal plane detectors, as well as the orientation of magnetic fields with respect to the equipment. With the exception of a few constraining surfaces which are discussed below, the model of the equipment is in agreement with the best known blueprints, "as-built drawings", and recent measurements. This was a major job taking almost four months to complete.

**Systematic effect of uncertainty in incident beam direction**

As discussed above, the incident beam direction can be determined to within ±0.10 mrad. The systematic effect of this on $A_{fb}$ was expected to be small and with the GEANT simulation of the experiment in good agreement with reality an investigation was carried out to quantify this effect. Nine GEANT runs were generated filling a 3 × 3 parameter space of angle offset vs. $A_1/A_0$. The inputs to the GEANT run at the centre of this 3 × 3 space were nominal (incident angle = 3.5 mrad, $A_1/A_0$ = 0.00%); the step size in the incident angle was ±1.0 mrad and that of $A_1/A_0$ was ±1.00%. Each run had 2.8 million events in it. These runs were compared to a statistically independent nominal run and the resulting $\chi^2$ space analyzed. The error matrix from this indicated that the correlated uncertainty in $A_1/A_0$ due to an uncertainty in the incident angle is ±0.06%/mrad. Thus, the systematic effect on $A_{fb}$ due to the uncertainty in the incident beam angle is $\pm 0.6 \times 10^{-4}$.

**Minimization of a three dimensional space**

As a test of the simulation and the $\chi^2$ minimization procedure, a 3 × 3 × 3 parameter space was generated, the 27 runs compared to the data of a single $np \rightarrow d\pi^0$ cycle, and a $\chi^2$ minimum found. The parameters of this test were the incident beam energy, momentum of the central ray of SASP, and target thickness. The nominal values for the simulation were taken from the data: the beam energy was extracted from the maximum lab scattering angle and found to be 279.755 MeV, a target thickness of 20.44 mm was determined from the centroid of H0 calibration data and target temperature of that cycle, and the magnetic fields of SASP were set to a central momentum of 711.425 MeV/c. Step sizes in the simulation were ±0.5 MeV in beam energy, ±2.0 mm in target thickness, and ±2% in central momentum. The three dimensional minimization found a strong correlation in (target thickness, $p_0$) space and a consequently larger $\sigma(p_0)$. This was tested by manually zeroing the $\chi^2$ (target thickness, $p_0$) partial derivatives. While the values of the parameters listed in Table VII are in good agreement and the $\chi^2$/dof is very close to one, obvious disagreements between the data and simulation can be seen in Fig. 37. The source of this disagreement is thought to be an incorrect description of the SASP acceptance, which is described below.

Table VII. Results of a 3-D minimization and data.

| | 3D minimization | Data |
|---|---|---|
| $LH_2$ (mm) | 19.23 ± 0.12 | 20.44 ± 0.66 |
| $E_{beam}$ (MeV) | 279.806 ± 0.005 | 279.755 ± 0.020 |
| $p_0$ (MeV/c) | 713.405 ± 0.054 | 711.425 ± 0.035 |
| $\chi^2$/dof | 1.116 | |

**Input from other mechanisms**

This experiment requires a knowledge of the energy dependence of deuteron reaction losses in the range of 100 to 150 MeV, with an accuracy of order 0.1%, for input to the GEANT simulation. The GEANT subroutine GHEISHA treats deuterons as "heavy fragments" and is improper in that (1) the total cross sections are purely geometric "black disk" with no energy dependence, (2) no inelastic scattering occurs for kinetic energies above 100 MeV, and (3) below 100 MeV the relative cross sections for various reaction channels seem to be chosen purely on the basis of reaction Q-values and

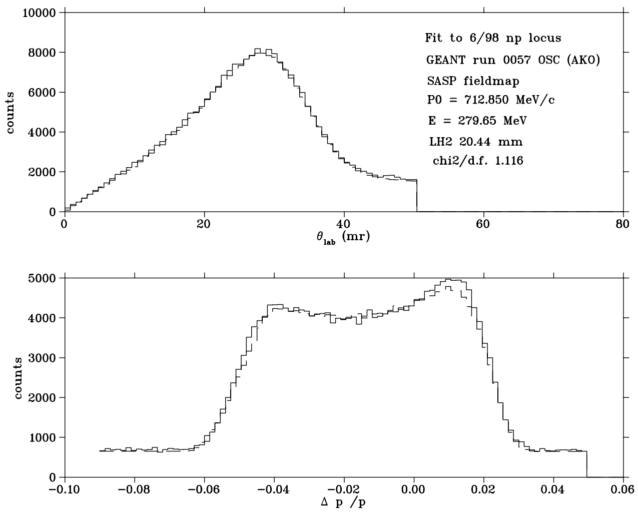


Fig. 37. Projections of the kinematic locus of one $np \to d\pi^0$ cycle and a GEANT simulation using target thickness, beam energy, and $p_0$ values that minimize $\chi^2$.

the energy/angle distributions based solely on phase space.

Data on total reaction cross sections of deuterons on various nuclei, of elastic scattering of deuterons by $^1$H, $^{12}$C and $^{16}$O, as well as a model (due to Glauber) for deuteron breakup cross sections have been incorporated into lookup tables which the GEANT simulation uses. The simulation gives good agreement with measured reaction rates and the energy dependence of those rates. An analysis with a simple Monte Carlo indicates that an uncertainty of 50% in the momentum dependence of these rates will produce a systematic effect of $\pm 14 \times 10^{-4}$ on $A_{fb}$. The collaboration is searching the literature for more precise deuteron cross section measurements so we can meet our precision goal of $\pm 10 \times 10^{-4}$.

**Model of SASP acceptance**

The acceptance of SASP is a complicated function of the position and angle at which the deuteron is produced and its momentum ($X_i,\ \theta_i,\ Y_i,\ \phi_i$, and $\delta$). Describing this acceptance properly requires an accurate model of the magnetic fields in SASP because (1) deuterons can collide with interior surfaces of SASP and be lost from the locus and (2) the reconstructed momentum variable, which is a function of the focal plane variables $X_f$ and $\theta_f$, may be distorted in a momentum dependent way by an inaccurate model. The SASP dipole has a non-uniform gap and magnetic saturation causes the field to sag at the high-field (small gap) region, relative to ideal. Experiment 704 took data with the spectrometer powered to a field that lies between that of the comprehensive field maps. We now have four descriptions of the SASP dipole: (1) a model based on RAYTRACE, (2) the 875 A map scaled to 907 A, (3) the 950 A map scaled to 907 A, and (4) a linear combination of the two maps that correspond to 907 A. The map-based models were developed in the latter part of 2000.

Robust tests of the simulation must involve comparison of the model and data for observables that are independent of $A_{fb}$. To that end, two sets of acceptance calibration data were taken, namely (1) the measurements of the SASP dispersion, taken with high resolution $^{208}$Pb$(p,p')$ (small beamspot on target), and (2) measurements of $(n,p)$ elastic scattering (large secondary beam on target). The measurements of $np$ elastic scattering were done with fixed magnet settings and three different incident beam energies to produce protons with $\delta = -4,\ 0,\ +4\%$ and thereby span the momentum distribution of the $np \to d\pi^0$ deuterons.

The $^{208}$Pb$(p,p')$ calibration data were taken with constant fields on the SASP magnets and different beam energies so as to also span the momentum range of interest. Extracting the dependence of the projectile momentum on its detected position in the focal plane detectors ($X_F$) from these data led to a third order function of $X_F$:

$$\delta = \left(\frac{X_F}{P_1}\right)\left[1 + \frac{X_F}{P_2}\left(1 + \frac{X_F}{P_3}\right)\right],$$

where $P_i$ are the coefficients of the fit. We see a discrepancy of $\sim$17% between the $P_2$ extracted from this calibration data and that extracted from a simulation using the scaled 875 A map. The other coefficients from the simulation are in good agreement with those from data or have no effect on $A_{fb}$. We believe the description of the SASP magnetic fields will not improve greatly and there will still be a discrepancy between the value it gives for $P_1$ and that of the data. Consequently we will treat the simulation as a "different spectrometer" but be consistent in the analysis techniques used. Thus, we will use the techniques developed to determine the functional form of $\delta = \delta(X_F)$ from the $^{208}$Pb$(p,p')$ data in a simulation with the best model of the SASP magnetic fields to determine a similar function for analysis of simulated data.

Investigation of the dependence of the focal plane proton peak centroids and widths (from the $np$ elastic scattering data) on the position or scattering angle at the target reveals good agreement between data and simulation if analysis is restricted to a small acceptance volume. However, some discrepancies do exist if the full acceptance employed in the analysis is used. These discrepancies could result from a mismatch in the SASP optical parameters. Reducing any differences between the measured and GEANT $np$ elastic matrix elements may increase the range of acceptance that we can safely use.

Comparisons of matrix elements from $np$ elastic data and those from simulations with models (1) and (2) above, for all three momentum values, show better overall agreement with model (2). The matrix elements from the RAYTRACE model show discrepancies with data that range from a few to 20%, whereas those from the 875 A map range from 0 to 8%. The increased agreement with the field map is especially pronounced for the $< X_f|X_i >$ matrix element which must be described well if we are to use most of the large spatial extent of the target. The precision of the matrix element description is at the 5% level. GEANT simulations that used $< X_f|X_i >$ correlations differing by 6% yielded $A_{fb}$ values that differed by $1.4 \times 10^{-4}$.

To investigate the momentum dependent effects, projections of $Y_i$ and $\phi_i$ have been made for slices in $X_i$ and $\theta_i$ and ratios of these distributions made for data vs. GEANT and for the –4% vs. +4% momentum sets. The basic features of these ratios are understood in terms of the focusing action of the SASP entrance quads, Q1 and Q2. For "onside" rays, those in which $Y_i$ and $\phi_i$ have the same sign, the –4% rays are defocused more strongly by Q1 than are the +4% rays and they tend to be lost at the exit of Q1. For "offside" rays, those which have opposite signs for $Y_i$ and $\phi_i$, the differential losses occur at the exit of Q2, where it is the +4% rays which tend to be lost more due to less defocusing in Q2. These features appear in both data and GEANT but GEANT does not accurately represent the shoulder region where the acceptance in $\phi_i$ begins to fall. The inner surfaces of the quads are complex and modelled consistently with the most reliable blueprints. It is unlikely that the model of these magnetic elements will improve in a reasonable amount of time. Consequently, we have determined cuts which exclude those portions of the acceptance that cannot be adequately modelled. These cuts are on target position and angle and define regions of uniform acceptance. Much effort was directed at developing a method to find the flat acceptance range in an automated and unbiased manner. Fits were done for three ranges in $\theta_i$ and only a weak dependence on $\theta_i$ was found. The application of these acceptance defining cuts from $np$ elastic data on the $np \to d\pi^0$ data are found in Table VIII; a similar procedure remains to be done on the GEANT simulations.

Table VIII. Effect of tabular cuts on $np \to d\pi^0$ data.

| Cut | Total events in locus $\times 10^6$ | Deuterons in locus $\times 10^6$ | Fraction |
|---|---|---|---|
| $X_i,\ Y_i$ | 14.19 | 7.78 | 100.0% |
| $+\ \theta_i$ | 11.38 | 7.34 | 94.3 |
| $+\ \phi_i$ | 9.49 | 6.34 | 90.07 |

**Other activities**

Near threshold the maximum deuteron scattering angle in the lab is strongly dependent on the beam energy. Relative beam energies have been extracted from the maximum deuteron scattering angle for all cycles. In these data, the uncertainty in that angle is $\pm$ 0.1 mrad which leads to an uncertainty in the average beam energy of $\pm$ 20 keV. Target thicknesses for all cycles have been extracted from centroids of H0 running and $np$ elastic scattering. The thicknesses have been corrected for target temperature variations.

The last pass of the analysis produces efficiency profiles for the detectors; these exist for all $np \to d\pi^0$ data. Typically the VDC planes are ∼99% efficient. These efficiency distributions vary across the VDC planes and lead to false values of $A_{fb}$ that range from –0.000530 $\pm$ 0.000085 to +0.000280 with a comparable uncertainty. While these instrumental asymmetries are small, they are significant on the anticipated scale of the observable and must be included in the simulation. Code to use these efficiency profiles has been added to the simulation.

To reduce the possibility of psychological bias in matching simulation to data, a "black box" subroutine has been added to the simulation. This routine adds a (hidden) offset to the $A_1/A_0$ asymmetry parameter used to set up the $np \to d\pi^0$ generator in the simulation. A member of the collaboration not involved in simulation development selected the offsets from a predetermined range, compiled the subroutine on all simulation farms, mailed the source code to two people outside the collaboration, and deleted the source code.

**Final steps**

As described below, $A_{fb}$ can be determined from the $np \to d\pi^0$ and $np$ elastic scattering data. The $pp \to d\pi^+$ data might possibly be used to constrain the deuteron reaction losses. However, these data may be too difficult to model accurately, due to the momentum correlated charged particle backgrounds. These and other uncertainties may make the reaction loss information obtained from $pp \to d\pi^+$ of limited precision and, therefore, limited usefulness. With the human resources for this experiment being very limited we have decided to use the $np \to d\pi^0$ and $np$ elastic scattering data to determine $A_{fb}$ and return to the $pp \to d\pi^+$ data and simulation at a later date.

**Determine acceptance**

The $np$ elastic scattering data provide the best means to determine the acceptance in that the incident beam of this reaction fills the target parameter space in a way that is similar to that of the $np \to d\pi^0$ reaction. Consequently the simulation must agree with these data. Improvements to the description of the SASP magnetic fields are (1) determine $\delta = \delta(X_F)$ for the simulation and (2) remove aberrative effects from the simulation using the same techniques that are used for the data. We will then finalize the cuts that define uniform acceptance in the $np$ elastic scattering data and in the magnetic field based simulation, and apply these to the $np \rightarrow d\pi^0$ data. A robust test of the acceptance will be simulation vs. data comparisons of $A_1/A_0$ extracted from target subspaces, e.g. $A_1/A_0$ from $X_i > 0$ and from $X_i < 0$. If the difference between simulated and measured values of $A_1/A_0$ is larger than can be expected from statistics, the tightness and ranges of the acceptance cuts will have to be changed so as to bring the simulation into agreement with the data.

#### Determine systematic sensitivities

Simulation vs. simulation comparisons will be carried out to determine how strongly the experimental parameters are correlated with $A_1/A_0$. For each parameter this will involve simulating kinematic locus scatter plots for a $3 \times 3$ grid of the experimental parameter vs. $A_1/A_0$, calculating the $\chi^2$ of those nine plots when compared to a plot simulated with nominal values, and fitting the $\chi^2$ space. The correlation of $A_1/A_0$ with the experimental parameter will be obtained from the error matrix based on the curvature of the $\chi^2$ space. Combining this correlation with the uncertainty in the parameter gives the systematic sensitivity of $A_1/A_0$. Note that the uncertainty in the parameter comes from a separate determination and not from the $\chi^2$ minimization. We are currently going through this procedure for ten different parameters; the results for the sensitivity to the incident beam direction are discussed above.

#### Determine correlated parameters

The effects of some of the parameters are correlated and they will have to be treated differently. This step will also involve simulation vs. simulation tests, however this time the $\chi^2$ minimization and correlation studies will be done in parameter$_i$ vs. parameter$_j$ space, where $i$ and $j$ indicate correlated parameters. If necessary, three parameters may have to be fit simultaneously.

#### Obtain $A_1/A_0$

At this point all the inputs to the simulation will be fixed except for $p_0$, the average nominal beam energy, and $A_1/A_0$. If there are other parameters which cannot be constrained by an independent determination, they will have to be added to the fit. Note that for each parameter added to the fit, a dimension is added to the $\chi^2$ space and the number of "grid" points increases dramatically. The whole data set will then be simulated with appropriate weightings of target thickness, relative beam energy, and efficiency profiles for each cycle. $A_1/A_0$ will be determined by minimizing $\chi^2$ over this multidimensional parameter space. Correcting this value of $A_1/A_0$ for the offset from the "black box" subroutine will yield $A_{fb}$.

### Experiment 715
### Weak interaction symmetries in $\beta^+$ decay of optically trapped $^{37,38\mathrm{m}}$K

*(J.A. Behr, TRIUMF; K.P. Jackson, TRIUMF/SFU)*

#### Summary

The $\beta^+$-$\nu$ correlation measurement in the $0^+ \rightarrow 0^+$ Fermi decay of $^{38\mathrm{m}}$K has collected data this August and October with statistical error on the angular correlation coefficient $a$ of $\approx 0.3\%$. The electric field apparatus was completely redesigned and rebuilt, and a successful external review was held. Our intention now is to publish our preliminary number based on the ISAC April, 1999 data as soon as possible. The final answer will be published when the analysis is complete. As the new geometry is cleaner, we hope to extend the analysis to as low a $\beta$ energy as possible. This will enable simultaneous extraction of limits on $a$ and the Fierz interference term $b$m/E from a single experiment; something which only we can do.

The spin-polarized program has made considerable progress. Vector polarization of $P=< M_I > \approx 90\%$ in stable $^{41}$K was demonstrated in the off-line lab with a simple atomic probe, in a simplified version of what is eventually planned. The apparatus was moved to the on-line lab. Four shifts were spent in a test run to evaluate nuclear detection hardware, using the present chamber geometry to explore limitations to assist design of the next apparatus. Approximately 60% nuclear polarization of $^{37}$K was achieved. The goal was to attempt a first time-reversal violating $D$ coefficient test; although this was not possible, much was learned about potential systematic effects.

### Scalar search in $^{38\mathrm{m}}$K $\beta^+$-$\nu$ correlation

#### Present status of other experiments and theory

In addition to the published work in the $\beta$-delayed $p$ emission of $^{32}$Ar [Adelberger *et al.*, Phys. Rev. Lett. **83**, 1299 (1999)], which achieved $\tilde{a}_{\mathrm{Fermi}} = \frac{a}{1+b\frac{m_e}{E}} = 0.9989 \pm 0.0052 \pm 0.0039$, there are two other experiments approaching publication and several other proposals. A Dubna/Orsay/Louvain collaboration has an experiment on the $\gamma$-ray Doppler shift of $^{18}$Ne and a published preliminary result with an error on $a$ of 0.10 [Egorov *et al.*, Nucl. Phys. **A621**, 745 (1997)], and is close to publishing a result with a statistical error of 0.01 on $a$. A Dubna/Louvain/PSI experiment using a forbidden transition in $\mu$ capture on $^{16}$O says they will publish a number soon with a statistical error of 0.01 on $C_S$ (the above experiments are primarily sensitive to $C_S^2$), but with unknown and possibly large theoretical error.

In addition to the possibilites cited in the past of constraining the couplings and masses of elementary exchange bosons like a charged Higgs [Herczeg, in *Precision Tests of the Standard Electroweak Model*, P. Langacker, ed., p.786 (1994)], additional phenomenological motivation exists for constraining the parameters $C_S$ and $C'_S$. The Los Alamos Theory group can explain a possible excess of events at the tritium $\beta$ decay endpoint by an admixture of $\nu_e$ with a 5 eV $\nu$ and in addition a non-standard model interaction, either a right-handed vector interaction or a scalar interaction – in particular, constraints on scalars coupling to right-handed neutrinos are required [Stephenson *et al.*, Phys. Rev. **D61**, 093013 (2000)]. If the above limit of Adelberger *et al.* can be improved by a factor of three, that would rule out the scalar interaction explanation [Goldman, private communication].

To interpret the eventual result on $C_S$ and $C'_S$ in terms of exchange bosons, which couple to the quarks and leptons, a scalar form factor for the nucleon $g_S$=$<p|\bar{u}d|n>$ is needed. A compilation and evaluation of previous models gives values between 0.25 and 1.0 [Herczeg, *op. cit.*]. This quantity is related to form factors recently evaluated in lattice gauge theory [Liu *et al.*, Phys. Rev. **D59**, 112001 (1999)] by an isospin rotation, and the result is $|g_S| = 0.63 \pm 0.09$. The calculational method gives quantities such as $g_A$ in agreement with experiment to ≈10% [Woloshyn, private communication], and is therefore more than adequate for this purpose.

**Experiment details**

**Isotope production and trapping**

The ISAC production target is now pressed $CaZrO_3$ disks. The target was tested with as much as 2.5 $\mu$A proton beam. $1.5 \times 10^7$/s $^{38m}$K was delivered reliably for 4 weeks of running at 1.5 $\mu$A of proton beam. $6 \times 10^6$/s $^{37}$K was delivered for the 4 shift spin-polarized run.

No Dryfilm degradation was observed during these runs. 15 keV energy ion source operation proved to be difficult and unreproducible, presumably due to transmission problems through the separator. Diffusion of $^{37}$K was measured at 30 keV and compared to 15 keV; the percentage released was at most only 20% worse at 30 keV, so 30 keV was used.

**E field**

An error discovered in the electrostatic field calculation geometry resolved most of the E field error, reducing the discrepancy between measured and calculated field from 4% to < 1%. Nevertheless, we upgraded the apparatus to: 1) shield all ceramics and HV connections with conductors; 2) simplify the geometry to make the field more uniform to allow simpler ion trajectory reconstruction; 3) use lower-$Z$ glassy carbon electrodes to reduce backscattering and minimize eddy currents when switching B fields quickly for polarized experiments; 4) use high-$Z$ passive collimation to reduce straggled $\beta^+$s and $\beta^+$s from wall backgrounds. A top view of the new apparatus is shown in Fig. 38.

Assuming the trap position is given by the TOF of the neutral recoils (see below), the E field can be measured by the TOF of: the fastest recoils; photoionized atoms at rest; and a population of events where a $\beta^+$ hits the MCP, directing the recoils away from the MCP. The three measurements of the E field agree to within 5 V/cm out of 810 V/cm. The field is thus more uniform than the field used in April, 1999. The discrepancy with the 800 V/cm calculated field remains to be understood, but using this measured determination of the field lowers the estimated error in $a$ from the electric field to <0.2%.

**Absolute trap position from $Ar^0$: $Ar^-$ ?**

The measured value of the E field is strongly correlated with the trap position. The trap position is given most precisely by the TOF of the fastest neutrals. A 0.4 mm systematic error in trap position would explain the E field discrepancy. The presence of long-lived $Ar^-$ species would affect this leading edge. There is a known 250 ns lifetime $Ar^-$ metastable. To explore this, data were also taken at 400 V/cm field. A precise determination was made of the neutral recoil TOF spectra, with the trap in identical positions. The presence of long-lived $Ar^-$ species would be indicated by a difference from unity of the ratio of the TOF spectra. The

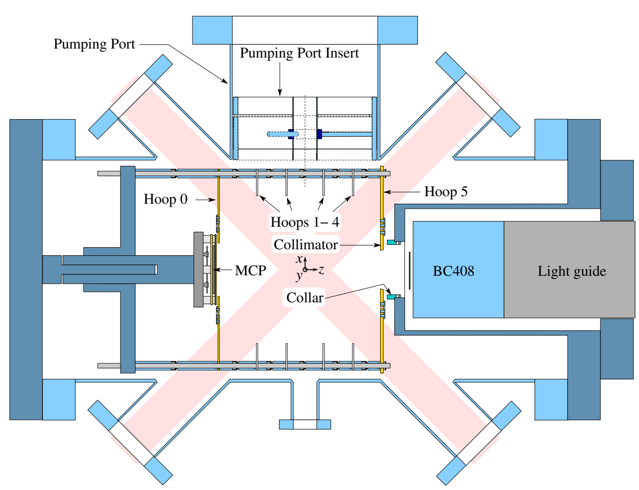


Fig. 38. Top view of new $\vec{E}$ field apparatus.

potential error in trap position was measured to be negligibly small.

#### Beta telescope

The $\beta^+$ telescope is a 0.46 mm thick double-sided Si strip detector with 24 × 24 1 mm wide strips for position sensitivity, backed by a 6.5 cm diameter × 5.5 cm long BC408 plastic scintillator with energy resolution 9.2% at 1.6 MeV. Calibration and characterization of this complex device were completed in the M.Sc. thesis of Dan Melconian, June, 2000.

#### MCP efficiency has been measured

We have measured the efficiency of the MCP as a function of energy in two ways. Probability of photoionization of $^{41}$K was measured, with results limited by systematic power fluctuations of the $N_2$ laser borrowed from the detector facility. This measurement implies the dependence is very similar to Ar at these energies. $^{38m}$K data were taken at electric fields of 765 and 735 V/cm. The resulting recoil energies span the range of interest for the 800 V/cm field where most of the data were taken, and the MCP efficiency is constant to a level that limits the error in $a$ to $< 0.2\%$.

Photoionization of radioactives also allows the size and position of the trap to be determined in the other 2 dimensions (in addition to the TOF axis), which is otherwise not possible to disentangle in the two CCD cameras.

#### Radiative corrections

We plan to get these from Glück in Budapest, who did similar calculations for $^{32}$Ar and has expressed keen interest in the past, now that our analysis is sufficiently advanced that we know what to ask for. The correction to $a$ was 0.3% in $^{32}$Ar. It is not needed for the preliminary publication, but must be included in the Monte Carlo for the final analysis. (Glück supplied a table to Adelberger *et al.*)

#### Ar$^0$ TOF spectra and MCP efficiency for neutral recoils

We measured the $^{37}$K $\beta$-$\nu$ correlation with better balanced MOT polarized beams, to try to achieve zero polarization. The goal was to test the MCP efficiency as a function of recoil energy for the Ar$^0$. The $^{37}$Ar ion data were consistent with the standard model, while the neutral data were badly inconsistent; suggesting an efficiency for neutrals dropping 25% per 100 eV. This is too large a correction to make in the $^{38m}$K data, so we will not use the Ar$^0$ data for the $^{38m}$K $\beta$-$\nu$ experiment.

### Error budget

The systematic errors are shown in Table IX.

Table IX. Systematic errors for $^{38m}$K as of December. $\vec{E}$ field error assumes trap position known from Ar$^0$ TOF (see text). Backgrounds from walls and $\beta^+$ backscattering are negligible.

| Error | Dec/99 | Dec/00 |
|---|---|---|
| $\vec{E}$ field | 0.5-2.0% | <0.2% |
| $E_{\beta+}$ detector: | | |
| Tail/total | 0.2% | 0.2% |
| 511 summing/total | 0.2% | 0.2% |
| Calibration nonlinearity | <0.5% | <0.25% |
| MCP Eff[$E_{Ar+}$] | <0.6% | < 0.2% |
| Sum systematics | <0.8% | <0.5% |
| Statistics | ≈0.8% | ≈ 0.3% |

### Fits to TOF spectra of Ar ion recoils

The fit to the Ar ion TOF spectra from April, 1999 data is shown in Fig. 39. This produces a preliminary result $\tilde{a} = 0.992 \pm 0.008$ (stat) $\pm$ 0.005 (syst).

### Experimental plans for spin-polarized observables

#### Physics motivation

We have listed in detail in the past the physics justification for the right-handed current experiments. We summarize here the physics justification for direct time-reversal violating measurements. These can be done without complete knowledge of the polarization.

The parity-even coefficient $D$ of the vector product $\vec{J}_N \cdot (\vec{p}_\beta \times \vec{p}_\nu)$ is the time-reversal odd correlation most naturally measured with our $\beta^+$-recoil coincidence techniques. A recent calculation of $D$ in the standard model predicts it to be at the $10^{-12}$ level [Herczeg and Khriplovich, Phys. Rev. **D56**, 80 (1997)]. The best experiments to date have set limits at $<6 \times 10^{-4}$ [Hallin *et al.*, Phys. Rev. Lett. **52**, 337 (1984)]. Thus any violation at experimentally foreseeable levels would be from new physics beyond the standard model.

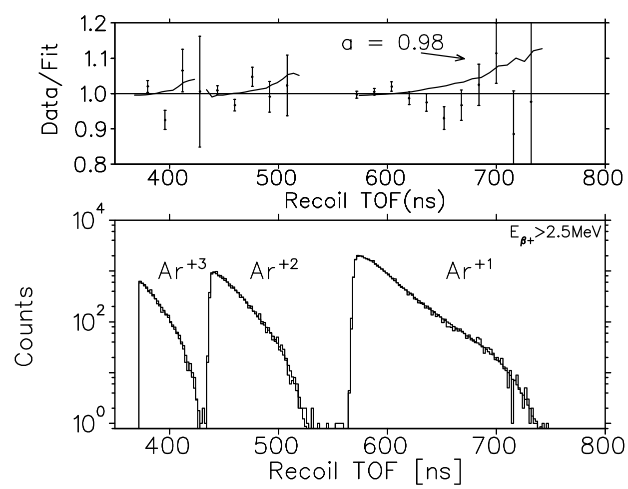


Fig. 39. Preliminary Monte Carlo fit to recoil $^{38}$Ar +1,+2,+3 TOF spectra, $E_{\beta+} > 2.5$ MeV.

Some possible contributions to $D$, such as leptoquarks, are *not* constrained by electric dipole moment experiments, while other contributions (from left-right symmetric models and exotic fermion models) are indirectly constrained by EDM experiments, although in a model-dependent fashion [Herczeg, in *Symmetries and Fundamental Interactions in Nuclei*, Haxton and Henley, eds. (World Scientific, Singapore, 1995), p.111]. Final state effects that mimic time reversal are smaller in $^{37}$K than in $^{19}$Ne by $\approx 2\times$, on average $\approx 1.0 \times 10^{-4}$, and they have an almost linear dependence on $E_{\beta+}$ which can be measured and tested [Holstein, Phys. Rev. **C5**, 1529 (1972)].

#### Off-line lab polarization progress

Polarization of $\geq 92\%$ of $^{41}$K was achieved in the off-line lab. Details are summarized in the Experimental Facilities section of this Annual Report.

#### First $^{37}$K polarization tests

A similar scheme was implemented in the on-line lab, with optical pumping light perpendicular to the detector axis. In the present chamber geometry, the optical pumping beam could not be retroreflected, and this limited the $^{41}$K polarization (this can be easily remedied by adding ports). Otherwise, this would be a possible geometry for a $D$ coefficient measurement.

The atoms are polarized along the $X$ direction; $\beta^+$s go along the fixed $Z$ direction; charged recoils can be measured going to + or $-Y$. The position dependence is measured in the MCP, and would shift as the polarization is flipped if there were a finite $D$ coefficient. The polarization can be monitored along the $X$ direction by looking at the recoil asymmetry, both in singles and in coincidence with the $\beta^+$; in both cases there is a large, calculable asymmetry.

This geometry provides a complete set of monitors for systematic errors. For example, the recoil singles – which will show no time-reversal violating effect – can be used to monitor unwanted residual polarization along the $Y$ axis. It may be possible to find a true polarization axis about which the recoil singles have no asymmetry, and look for a $D$ coefficient with the recoil coincidences about that axis.

The polarization was also monitored with $\beta^+$s in the double-sided silicon strip detector, as even though it is close to 90° it still has finite analyzing power and excellent statistics. In addition, we have demonstrated for $^{38m}$K that the MCP has double hits which are $\beta^+$'s followed by Ar recoils; that may eventually allow a critical check on $D$, as false $D$'s will have the same sign for $\beta$ telescope recoil coincidences as for MCP double hits, while the effect of a true $D$ coefficient will have opposite sign because the $\beta^+$ is in opposite directions.

Raw data are shown in Fig. 40, showing asymmetries in the $X$ and $Y$ directions. A clear, large asymmetry in the $X$ direction is generated in each case; unfortunately, a much smaller but still finite unwanted $Y$ asymmetry also exists. The recoils, together with the $\beta^+$ singles, indicate that between 50 and 70% nuclear polarization was achieved. We will attempt to find the polarization axis as outlined above, but it is clear that purer polarizations will be needed for real experiments.

#### Circularly polarized FORT

There are a variety of neutral atom traps that may provide better polarization in the future. In particular, a spin-polarized far-off resonance dipole force trap under development (by Weiman) traps atoms in one magnetic substate. In principle, this trapping technique has little dependence on the quality of circularly polarized light [Cho, J. Korean Phys. Soc. **30**, 373 (1997)], and is free of depolarizing quadrupole B fields. Recent progress has been made in loading this trap efficiently [Corwin *et al.*, Phys. Rev. Lett. **83**, 1311 (1999)]. Our intention is to begin development of this technology in spring, 2001, using an existing Ar ion laser and standing-wave Ti::Sapph.

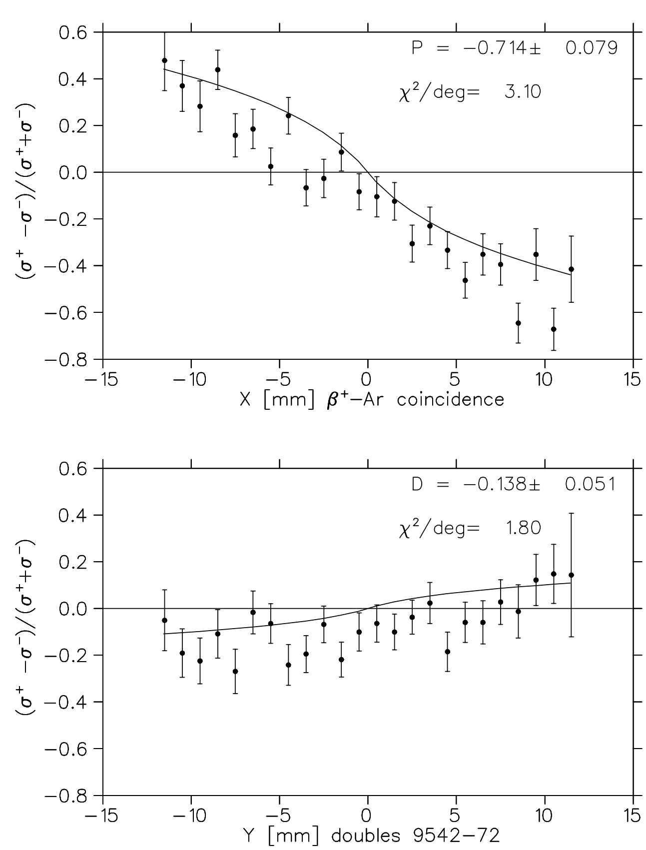


Fig. 40. Asymmetry in MCP position for $\beta^+$-Ar coincidence.

**Experiment 741**
**Beta-delayed proton decay of $^{17}$Ne to $\alpha$-emitting states in $^{16}$O**
*(J.D. King, Toronto)*

The goal of this experiment is to obtain an $\alpha$-particle spectrum from the break-up of $^{16}$O following the $\beta$-delayed proton decay of $^{17}$Ne, and to use this spectrum to reduce the uncertainty in the $^{12}$C$(\alpha,\gamma)^{16}$O reaction rate, which is of prime importance in determining the ratio of $^{16}$O to $^{12}$C at the end of helium burning in stars. In Expt. 589 we measured the $\alpha$-particle spectrum from the break-up of $^{16}$O following the $\beta$ decay of $^{16}$N. Through simultaneous $R$- and $K$-matrix fits to this spectrum, to the $^{12}$C$(\alpha,\gamma)^{16}$O data sets, and to $^{12}$C$(\alpha,\alpha)$ scattering data, we were able to reduce considerably the uncertainty in the $E1$ component of the astrophysical $S$-factor for the $^{12}$C$(\alpha,\gamma)^{16}$O reaction, which is determined primarily by the tail of the sub-threshold $1^-$ state at 7.117 MeV. Since the $2^+$ state at 6.917 MeV is not populated in the decay of $^{16}$N, the effect of the tail of this sub-threshold state on the $E2$ component was not determined, and a very large uncertainty in this component, which could be as large as the $E1$, still exists. However, $2^+$ states in $^{16}$O are populated in the $\beta$-delayed proton decay of $^{17}$Ne and the feasibility of using this decay is being explored in this experiment.

In last year's Annual Report we described the preliminary analysis of data from the runs of November and December, 1998, in which a high-quality time-of-flight (TOF) proton spectrum was obtained, and of the data from a run in April, 1999, in which a high-quality alpha spectrum was obtained using the ratio-cut technique. These spectra have now been fitted using Breit-Wigner line shapes for the excited states of $^{17}$F, and complete decay schemes for $\beta$- and $\beta$-delayed-particle decay of $^{17}$Ne have been obtained. Also, using $R$-matrix techniques, the spectra from $\beta$-delayed $p\alpha$ and $\alpha p$ decay through the isobaric analogue state (IAS) in $^{17}$F at 11.193 MeV have been fitted and branching ratios for this decay mode have been extracted. Finally, an experimental arrangement which would allow an independent determination of the $S$-factor for the $E1$ component of the $^{12}$C$(\alpha,\gamma)^{16}$O reaction is outlined.

**Branching ratios**

Branching ratios (BRs) for the decay of several excited states in $^{17}$F via proton emission to the 6.130, 6.917 and 7.117 MeV states in $^{16}$O have been obtained via proton-gamma coincidence measurements [King *et al.*, Nucl. Phys. **A621**, 169c (1997)]. However, those BRs were incomplete as they did not include proton decay to the $0^+$ state at 6.049 MeV or to the ground state. Also they did not include BRs for $\alpha$ decay. In the 1999 Annual Report, we displayed complete proton and $\alpha$-decay spectra and indicated that detailed analysis of the spectra using Breit-Wigner fitting techniques was in progress. These fits have now been completed (see Fig. 41) and a complete set of proton and $\alpha$ BRs for the decay of excited states in $^{17}$F has been obtained. The fit functions in Fig. 41 include 58 proton transitions and 13 $\alpha$ transitions. The decay is complex, as illustrated in Fig. 42, and space does not permit the display of particle-decay BRs here.

Beta-decay BRs were deduced from these results and are shown in Table X, where the present results are compared with the two previous studies. In general, BRs to excited states in $^{17}$F that are able to decay to excited states in $^{16}$O are much higher than previously reported, since the present study has been sensitive to decay modes missed in the previous work. The BRs of states that can decay only to the ground state of $^{16}$O are, accordingly, much lower.

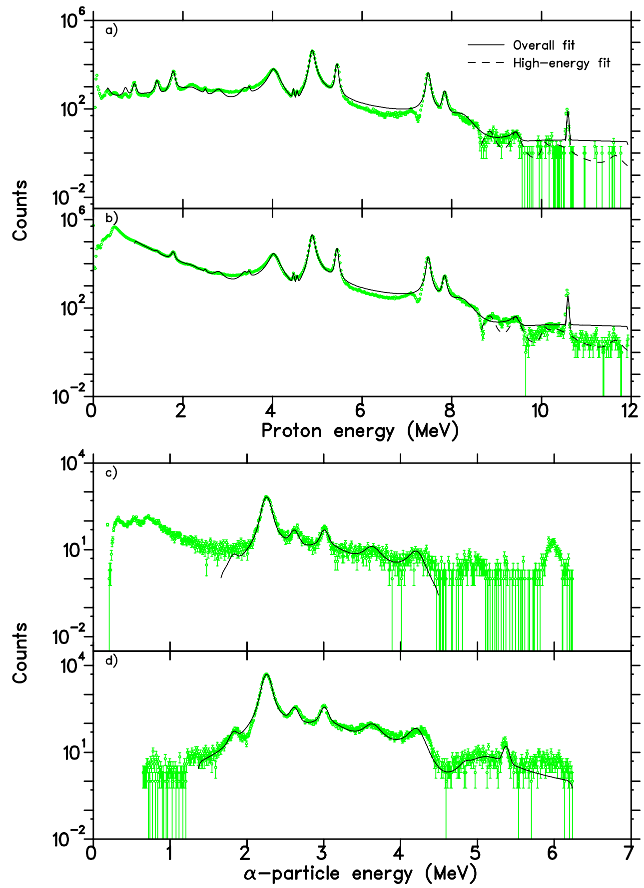


Fig. 41. Results of the simultaneous fits to a) proton TOF, b) ungated particle, c) $\alpha$-particle TOF and d) $\alpha$-particle, ratio-cut spectra.

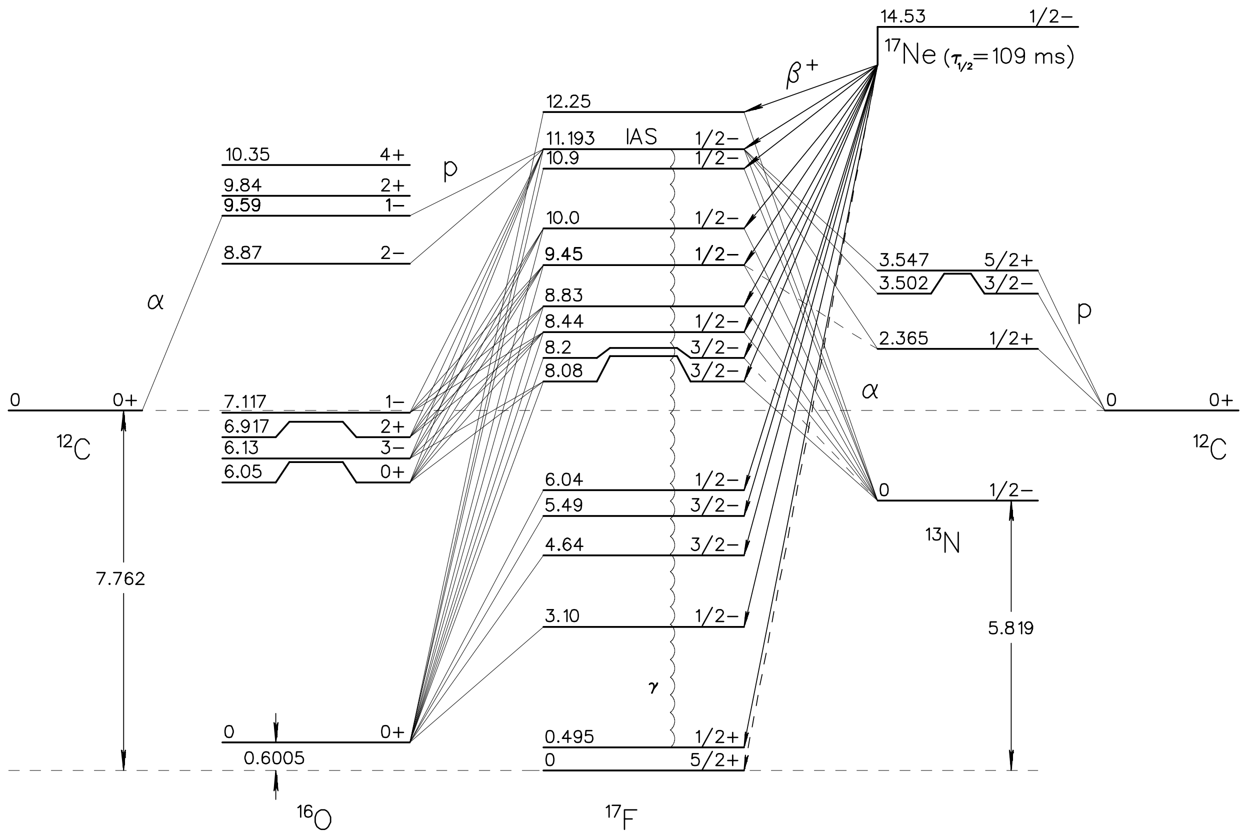


Fig. 42. Decay scheme for the $\beta$-delayed particle decay of $^{17}$Ne.

Table X. Branching ratios for the beta decay of $^{17}$Ne.

| Final state ($^{17}$F) | Branching ratios (%) Ref. [1][a] | Ref. [2][b] | This work |
|---|---|---|---|
| 12.25 | — | $0.001 \pm 0.0006$ | $0.0019 \pm 0.0004$ |
| IAS | $0.71^{+10}_{-0.05}$ | $0.64 \pm 0.14$ | $0.763 \pm 0.034$ |
| 10.91 | — | $0.016 \pm 0.006$ | $1.791 \pm 0.031$ |
| 10.66 | — | $0.007 \pm 0.004$ | $2.159 \pm 0.041$ |
| 10.029 | — | $0.7 \pm 0.3$ | $1.354 \pm 0.016$ |
| 9.45 | $0.54 \pm 0.05$[c] | $0.6 \pm 0.2$ | $2.502 \pm 0.034$ |
| 8.825 | $1.9 \pm 0.06$ | — | $7.344 \pm 0.081$ |
| 8.436 | $6.51 \pm 0.26$ | $4 \pm 0.9$ | $7.682 \pm 0.079$ |
| 8.2 | — | $1.7 \pm 0.3$ | $3.61 \pm 0.17$ |
| 8.075 | $6.83 \pm 0.11$ | $7.3 \pm 0.9$ | $5.789 \pm 0.043$ |
| 6.037 | $10.6 \pm 0.2$ | $7.8 \pm 0.2$ | $6.823 \pm 0.032$ |
| 5.488 | $54 \pm 0.7$ | $59.16 \pm 0.4$ | $45.02 \pm 0.19$ |
| 4.64 | $16.2 \pm 0.7$ | $16.54 \pm 0.14$ | $12.873 \pm 0.076$ |
| 3.104 | $0.48 \pm 0.07$ | $0.10^{+0.03}_{-0.01}$ | $0.1406 \pm 0.0051$ |
| 0.495 | $1.1 \pm 0.5$[d] | $0.76 \pm 0.13$[e] | $1.61 \pm 0.16$[f] |
| 0 | $0.53 \pm 0.16$[d] | | $< 0.55 \pm 0.18$[g] |

[a]Hardy *et al.*, Phys. Rev. **C3**, 700 (1971).

[b]Borge *et al.*, Nucl. Phys. **A490**, 287 (1988).

[c]From the assignment of an observed proton group at 2.825 MeV in Ref. [1] to the 9.45 MeV state in $^{17}$F.

[d]Calculated by comparison with the mirror decay of $^{17}$N [1].

[e]Calculated in Ref. [2].

[f]From Borge *et al.*, Phys. Lett. **B317**, 25 (1993) and Ozawa *et al.*, J. Phys. G: Nucl. Phys. **24**, 143 (1998).

[g]From Millener, Phys. Rev. **C55**, R1633 (1997).

### *R*-matrix fits

In the 1998 and 1999 Annual Reports, we presented $\alpha$-particle spectra from the $\beta$-delayed $p\alpha$ and $\alpha p$ decay of $^{17}$Ne through the IAS of $^{17}$F. An $R$-matrix analysis of the spectrum (shown in Fig. 43) has been carried out and branching ratios for this exotic decay have been obtained.

The single-channel, single-level $R$-matrix formula

$$N_\lambda(E) = \frac{P_i \Gamma_f}{(E_\lambda - E + \Delta_\lambda)^2 + (\Gamma_f/2)^2}$$

was used [Chow, Ph.D. thesis (unpublished, 2000)] to obtain the energy spectrum of the intermediate states for the three observed 3-particle decay channels of the IAS shown in Fig. 43. In this equation $P_i$ is the penetrability of the feeding channel, $\Gamma_f$ is the width of the exit channel obtained from

$$\Gamma_f = 2 P_f \gamma_\lambda^2,$$

where $P_f$ is the penetrability of the decay channel and $\gamma_\lambda^2$ is the reduced width belonging to the state $\lambda$, and $\lambda$ labels the three intermediate states $^{16}$O(9.59), $^{16}$N(2.37), and $^{16}$N(3.50/3.55). The quantity $\Delta_\lambda$ is the level shift defined by

$$\Delta_\lambda = -[S(E) - b]\gamma_\lambda^2,$$

where $S(E)$ is the shift factor and $b$ is the boundary condition.

This $R$-matrix expression was used in an algorithm to generate the particle spectra for the three decay channels which were then fitted to the experimental $\alpha$ spectrum as shown in Fig. 43. The fit resulted in the BRs shown in the figure for the decay of the IAS to these three states relative to the BR for the decay of the IAS to the 7.117 MeV state in $^{16}$O which is set to 100.

**Spectrum showing interference between $1^-$ states**

The discovery of a decay of the IAS to the 9.59 MeV state in $^{16}$O [Chow *et al.*, Phys. Rev. C**57**, R475 (1998)] suggested to us that, by using the $\beta$-delayed proton decay of $^{17}$Ne in an experiment similar in principle to the case of $^{16}$N decay [Azuma *et al.*, Phys. Rev. C**50**, 1194 (1994)] we might obtain an additional constraint on the $E1$ component of the $^{12}$C$(\alpha,\gamma)^{16}$O reaction. Instead of being populated by a $\beta$ decay as in the case of $^{16}$N, the $^{16}$O states are populated by a proton decay in the case of $^{17}$Ne. The difference in the feeding channel makes the case of $^{17}$Ne more complicated, and the experiment much more challenging, due to the involvement of 3-body kinematics.

The interference between the IAS$\rightarrow^{16}$O(9.59)+$p$ and the IAS$\rightarrow^{16}$O(7.117)+$p$ channels has been studied by means of a single-channel, two-level $R$-matrix calculation. The algorithm used for calculation of laboratory particle spectra is the same as that used for the BR calculation except that a single-channel, *2-level* $R$-matrix formula must be used to calculate the $\alpha$ energy spectrum from the decay of the $^{16}$O states. The expression is

$$N(E,\theta') = \left| \sum_{\ell=0,2} \frac{P_{p\ell}^{\frac{1}{2}} \sum_\lambda \frac{C'_{\lambda\ell}(\theta')\gamma_\lambda}{E_\lambda - E} P_\alpha^{\frac{1}{2}}}{1-(S_\alpha - b_\alpha + iP_\alpha)\sum_\lambda \frac{\gamma_{\lambda^2}}{E_\lambda - E}} \right|^2,$$

where

$$C'^{\,2}_{\lambda\ell}(\theta') = \mathcal{W}_{\lambda\ell}(\theta') C^2_{\lambda\ell}.$$

The $C_{\lambda\ell}$ are proton-feeding amplitudes and the $\mathcal{W}_{\lambda\ell}(\theta')$ are functions describing the angular correlation between the emitted protons and $\alpha$ particles; $\theta'$ is the angle between the $\alpha$ and recoil nucleus in the lab frame (and (180-$\theta'$) is the angle between the proton and $\alpha$). $P_{p\ell}$ and $P_\alpha$ are the proton and $\alpha$ penetrabilities, respectively. The reduced $\alpha$ widths obtained in the $^{16}$N experiment are used and the proton feeding parameters have been normalized such that

$$\int_0^{2\pi} (C'^{\,2}_{12} + C'^{\,2}_{20}) \sin\theta'\, d\theta' =$$

$$\int_0^{2\pi} [\mathcal{W}_{12}(\theta')C^2_{12} + \mathcal{W}_{20}(\theta')C^2_{20}] \sin\theta'\, d\theta' = 1.$$

Note that $C_{10}$ and $C_{22}$ are assumed to be negligibly small, i.e., a particular feeding channel only populates a single level ($\ell_p = 2$ to the 7.117 MeV state and $\ell_p = 0$ to the 9.59 MeV state).

**Proposed experiment**

A detailed study of possible configurations of a 3-detector system using one PIPS and two DSSD detectors was carried out using these $R$-matrix expressions in the algorithm mentioned above. The angles between detectors and the solid angles subtended by the detectors were varied in small incremental steps. The optimum configuration is shown in Fig. 44. Also shown in this figure are additional detectors positioned so that the entire array of 8 elements provides 6 combinations of 3 elements in the same optimum geometry. An experiment designed to accumulate an $\alpha$ spectrum following $\beta$-delayed proton decay of the IAS would employ two such arrays, one rotated at 20° about an axis in the beam plane through the collector foil and the second rotated through 20° in the opposite sense.

Two spectra that could be obtained with such a detector array are shown in Fig. 45. The dashed curve is the $\alpha$ spectrum due to decay only through the 9.59 MeV state. The effect of the tail of the 7.117 MeV state on the spectrum is shown by the simulated data points. The number of counts in each energy bin from this $R$-matrix Monte Carlo calculation has been randomized with a Gaussian distribution to simulate statistical fluctuations. The error bars represent a $1\sigma$

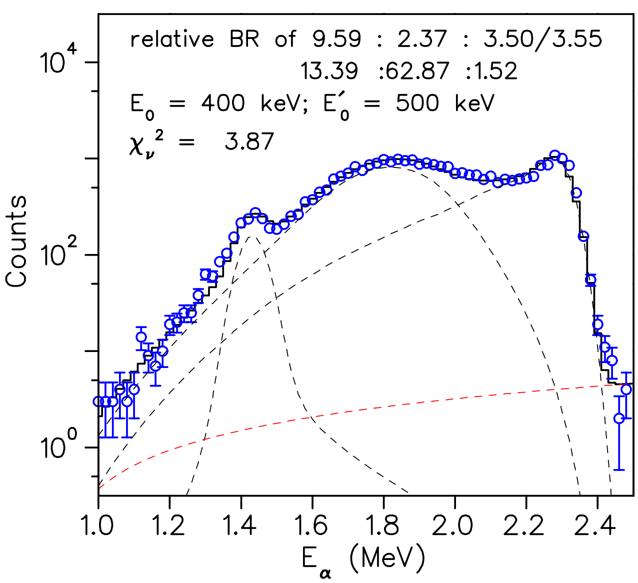


Fig. 43. $R$-matrix fit to the $\alpha$ spectrum resulting from $\beta$-delayed particle decay of $^{17}$Ne through the IAS.

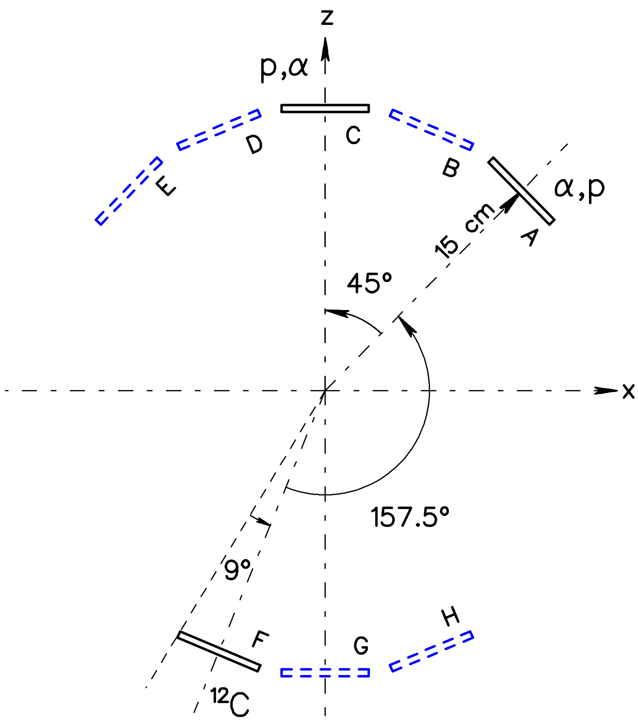

Fig. 44. Proposed detector configuration for detection of interference effects in the $\alpha$ spectrum following proton decay of the IAS.

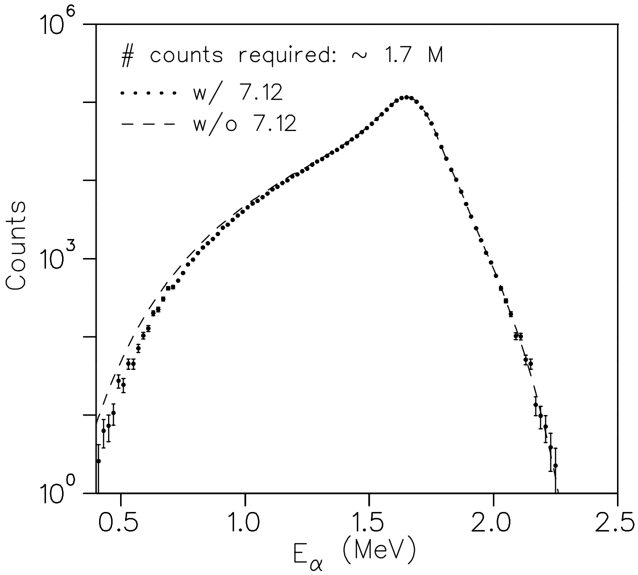

Fig. 45. Alpha spectrum expected from the detector configuration of Fig. 44 showing the effect of interference between the 7.117 and 9.59 MeV states in $^{16}$O.

uncertainty and the spectra have been convoluted with an experimental energy resolution of 40 keV. The total number of counts in the spectrum is about 1.7 million.

The maximum separation between the dashed curve and randomized data points of Fig. 45 is $8\sigma$ at about 900 keV with the separation falling to about $4\sigma$ at 500 keV and 1400 keV. The triple coincidence efficiency calculated for 3 detectors in the optimum geometry is $1.2 \times 10^{-5}$. For a $^{17}$Ne yield from ISAC of $10^8$ s$^{-1}$, the triple coincidence count rate would be 0.2 s$^{-1}$. The entire proposed system, with 12 sets in the same geometry, would detect about 2.4 counts s$^{-1}$. With the estimated ISAC $^{17}$Ne yield, the required number of counts could be obtained in 9 days. Yields of $^{17}$Ne of more than $10^5$ s$^{-1}$ were obtained at TISOL and the extrapolated ISAC yield seems reasonable.

## Experiment 778
## $\pi^{\pm}p$ differential cross sections in the region of Coulomb-nuclear interference

*(K.J. Raywood, TRIUMF; E.L. Mathie, Regina)*

The data-taking phase for Expt. 778 was completed during the high-intensity beam periods of 2000. The analysis phase is now under way, with the aim of providing a systematic set of differential cross sections for $\pi^{\pm}p$ elastic scattering at low energy and forward scattering angles. This is the region of Coulomb-nuclear interference (CNI) where Coulomb scattering interferes destructively (constructively) with $\pi^+p$ ($\pi^-p$) hadronic scattering amplitudes. This experiment is part of the CHAOS physics program whose goal is to test predictions and measure parameters of chiral perturbation theory. To this end, measurements have been made in the $\pi^{\pm}p$ sector of pion-induced pion production (Expt. 624) and elastic scattering analyzing powers (Expt. 560).

The data from this experiment will be used to determine, to a precision of a few per cent, the real part of the isospin-even scattering amplitude, D$^+$, at t = 0. This information is missing in the current partial wave analyses. Its inclusion will greatly improve the determination of the $\pi N$ scattering amplitudes. As a result, it will improve the determination of the $\pi N$ coupling constant, the $\pi N$ scattering lengths and the $\pi N$ $\Sigma$ term; all observables of crucial importance. The $\Sigma$ term, in particular, is a fundamental quantity. It is a direct measure of chiral symmetry breaking and can be obtained experimentally from the isospin-even $S$- and $P$-wave scattering lengths: $a^+_{0+}$ and $a^+_{1+}$.

The TRIUMF Cryogenic Targets group designed and constructed a planar cryogenic LH$_2$ target for this experiment. It was used with the same 12.5 mm thick cell that was used in the fall of 1999. Liquid hydrogen was maintained in the cell for periods of two to three weeks during foreground measurements. Following that, the target cell was emptied and background data were taken. The whole cycle was repeated at each energy and the target performed flawlessly throughout both high-intensity periods of 2000.

The CHAOS group was the first at TRIUMF to use the MIDAS data acquisition system. Early in 2000, several enhancements and bug fixes were made to the software by the primary author (Stefan Ritt, PSI) and Pierre Amaudruz of TRIUMF. The result was a very stable and flexible system that continues to improve and is now used by most TRIUMF experiments.

Throughout its history, the CHAOS programmable second-level trigger has been plagued by failures of some of its component commercially built modules. This problem arose again early in the first high-intensity period of the year. The decision was made to replace the functionality of the hardware with equivalent software running in the front-end processor. This was possible because of the significant increase in speed of the front-end processor compared with the one in use when the second-level trigger was first implemented. A third-level trigger was also designed and implemented for this experiment. It was based on fast ADC information from the $\pi/\mu$ range stack and a rejection of almost 50% was achieved. These improvements enabled Expt. 778 to run at a high data rate with a good live-time.

The CNI experiment received beam during both high-intensity periods of 2000. CHAOS was used to measure the angle and momentum of particles scattered from the liquid hydrogen target. The $\pi/\mu$ range stack was positioned to accept particles scattered at small angles. Its purpose was to distinguish true scatters from the large number of in-flight $\pi \to \mu$ decays. In the analysis, the information from the stack is fed to an appropriately trained neural network in order to identify pions and muons. At each beam energy, a measurement consisted of three parts at both polarities: foreground, background and neural network training (described in previous Annual Reports). Most of the data were collected in M13, but CHAOS was moved to M11 for the fall running period. The 39 MeV data set will be used as a consistency check as a full measurement was performed on both beam lines at that energy.

A summary of the amount of data collected at each energy and polarity is given in Table XI. The quantity $N_\pi$ is the live-time fraction of the total number of beam pions incident upon the target for the given configuration. It is tabulated for both foreground (fg) and background (bg) measurements. The quantity $\Delta Y(\theta_{s\text{-}p})$ is the statistical uncertainty of the yield in a 1° angular bin centred at the scattering angle of the minimum in the $\pi^+p$ cross section. The minimum is caused by the destructive interference between $S$-waves and $P$-waves and occurs at a laboratory angle of about 25° for 45 MeV and moves to larger angles at lower energies. Thus, the aim of achieving a 2% statistical uncertainty per 1° bin at the critical minimum in the cross section has been met at most energies.

Table XI. Summary of the data collected at each experimental configuration. The 57 MeV data were collected using beam line M11 and the 39 MeV data were collected using both M13 and M11. The remainder of the data were collected using M13. The 45 MeV values shown here include data taken at two target angles.

| $T_\pi$ (MeV) | Polarity | $N_\pi/10^{10}$ fg | bg | $\Delta Y(\theta_{s\text{-}p})$ (% /1° bin) |
|---|---|---|---|---|
| 15 | + | 5.1 | 1.9 | < 2 |
| 15 | − | 3.5 | 1.2 | 2.0 |
| 20 | + | 3.5 | 2.6 | 1.8 |
| 20 | − | 1.6 | 1.1 | 2.0 |
| 26 | + | 2.4 | 1.4 | 2.6 |
| 26 | − | 2.1 | 1.2 | 2.2 |
| 32 | + | 3.9 | 2.0 | 2.0 |
| 32 | − | 2.4 | 1.2 | 1.5 |
| 39 M13 | + | 5.4 | 3.6 | 2.0 |
| 39 M13 | − | 3.1 | 2.7 | 1.5 |
| 39 M11 | + | 2.2 | 1.9 | 3.1 |
| 39 M11 | − | 1.6 | 1.5 | 2.0 |
| 45 | + | 1.8 | 1.1 | 3.4 |
| 45 | − | 1.4 | 0.9 | 2.2 |
| 57 | + | 6.7 | 2.4 | 2.3 |
| 57 | − | 2.2 | 0.8 | 1.5 |

Though not shown in the table, data were also collected at 67 MeV but only at one polarity ($\pi^+$) and only at scattering angles larger than those accepted by the $\pi\mu$ stack. This measurement will provide a check on the target thickness as data were taken with two target angles. The energy was chosen in the hope that these data might also resolve a long-standing conflict in the global $\pi N$ database.

**Experiment 801**
**Studies of multi-phonon states via $\beta$-decay**
*(R.F. Casten, Yale)*

The atomic nucleus is a many-body system of strongly-interacting fermions and as such provides a fundamental "laboratory" for the study of collective excitations arising in a quantum mechanical many-body system. One of the most important issues is the relationship between single particle and collective degrees of freedom in such a system, which can be sensitively studied by investigating the properties of multi-phonon excitations of nuclear vibrational modes. Pauli exclusion effects severely restrict the freedom of individual nucleons to participate in multi-phonon collective vibrations, and it was long thought that multi-phonon excitations with unfragmented collectivity could not exist. In recent years, however, intact multi-phonon excitations have been found experimentally, and the very existence of these states provides a critical empirical test of models of nuclear structure.

Vibrational states arising from four-phonon or even five-phonon quadrupole excitations have been identified in spherical nuclei, but in deformed nuclei only a few solid candidates for states with even two phonons have been established, in $^{166,168}$Er and $^{232}$Th. There are a variety of challenges to the identification of multiple-phonon excitations, since these lie at energies approaching the pairing gap, above which a dense profusion of states of single-particle nature mask and admix with the collective states. A key question is thus whether the scarcity of observed multi-phonon states is due to genuine nonexistence of these states or simply to a lack of sufficiently sensitive data for their identification.

There is a straightforward signature of a two-phonon quadrupole excitation, namely that it is connected by a collective E2 transition matrix element to the one-phonon excitation of the same mode and by noncollective matrix elements to other lower states. In $\gamma$-ray intensity spectroscopy experiments, the accessible observables are ratios of matrix elements. A state with significant amplitude for a two-phonon $\gamma$ vibration ($K^\pi = 0^+$ or $4^+$) has a branching ratio

$$\frac{\langle K^\pi = 0^+_{2\gamma}/4^+_{2\gamma}||E2||K^\pi = 2^+_\gamma\rangle}{\langle K^\pi = 0^+_{2\gamma}/4^+_{2\gamma}||E2||K^\pi = 0^+_{\rm g.s.}\rangle} \gg 1$$

and a two-phonon $\beta$ excitation ($K^\pi = 0^+$) has

$$\frac{\langle K^\pi = 0^+_{2\beta}||E2||K^\pi = 0^+_\beta\rangle}{\langle K^\pi = 0^+_{2\beta}||E2||K^\pi = 0^+_{\rm g.s.}\rangle} \gg 1.$$

The aim of Expt. 801 is to extend the search for multi-phonon excitations in deformed nuclei to the neighbours of $^{166,168}$Er, by performing $\gamma$-ray spectroscopy of states populated in $\beta$-decay. The use of a compact configuration of large-volume Ge detectors, for efficent $\gamma$-$\gamma$ coincidence spectroscopy, coupled with the high intensity and high isotopic purity beams available at ISAC, provides much higher sensitivity than was available in the previous generation of experiments.

In June, an experiment to study $^{162}$Er was carried out at the ISAC GPS tape collector. The nuclei were produced through the decay $^{162}$Yb$\rightarrow^{162}$Tm$\rightarrow^{162}$Er, which populates several low-lying excited $K^\pi = 0^+$ bands. Beam nuclei from the ISAC separator were implanted into the GPS tape, and the tape was advanced to place a fresh source in front of the detectors at one hour intervals. Two 80%-efficiency coaxial Ge detectors were positioned 12 cm from the source location, oriented obliquely with respect to each other and separated by lead shielding to suppress background coincidence events due to $\beta^+$ annihilation photon pairs and Compton cross-scattering (Fig. 46). Data were acquired in event mode for off-line analysis. Both singles data ($1.5 \times 10^8$ events) and coincidence data ($6 \times 10^7$ events) were recorded.

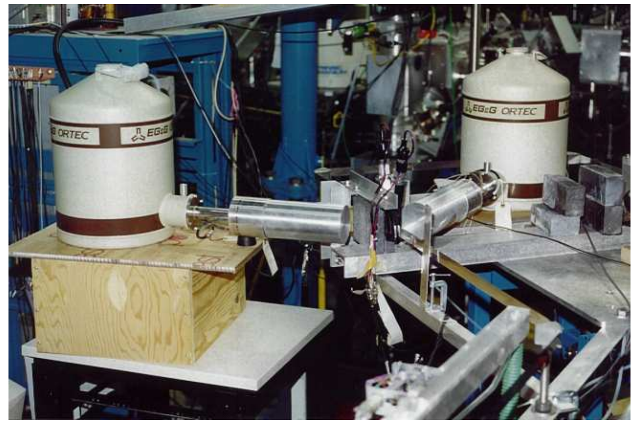


Fig. 46. Experimental set-up for Expt. 801 at the ISAC GPS tape collector system, with a compact configuration of two large-volume Ge detectors for $\gamma$-$\gamma$ spectroscopy.

Preliminary analysis provides the following branching ratios (and limits) for the two lowest excited $K^\pi = 0^+$ bands, with bandheads at $E(0^+_2) = 1087$ keV and $E(0^+_3) = 1420$ keV:

$$\begin{aligned}
\frac{\langle K^\pi = 0^+_3||E2||K^\pi = 0^+_2\rangle}{\langle K^\pi = 0^+_3||E2||K^\pi = 0^+_{\rm g.s.}\rangle} &< 4 \\
\frac{\langle K^\pi = 0^+_3||E2||K^\pi = 2^+_\gamma\rangle}{\langle K^\pi = 0^+_3||E2||K^\pi = 0^+_{\rm g.s.}\rangle} &= 3.5(2) \\
\frac{\langle K^\pi = 0^+_2||E2||K^\pi = 2^+_\gamma\rangle}{\langle K^\pi = 0^+_2||E2||K^\pi = 0^+_{\rm g.s.}\rangle} &< 3.
\end{aligned}$$

The level scheme is under revision on the basis of the coincidence data. The literature indicates a $J^\pi = 1, 2^+$ level at 1412 keV, nominally the second excited $K^\pi = 2^+$ bandhead, based upon the proposed placements of several transitions. However, coincidence analysis shows these placements to be incorrect, and there is thus no evidence for existence of the level. Continued analysis is under way.

This work was supported by the US DOE under grants DE-FG02-91ER-40609 and DE-FG02-88ER-40417.

**Experiment 812**
**Proposed study of the $^8$Li$(\alpha, n)^{11}$B reaction**
*(R.N. Boyd, Ohio State)*

The $^8$Li$(\alpha, n)^{11}$B reaction is being studied with an eye toward both big bang nucleosynthesis and the stellar r-process. In big bang nucleosynthesis, this reaction becomes important if there are density inhomogeneities during that epoch. If that is the case, the $^8$Li abundance can become large for some tens of seconds, during which time a large abundance of $^{11}$B can be made.

While other reactions ultimately lower the primordial abundance of $^{11}$B, during the time it is large it can undergo reactions to synthesize nuclei heavier than $^{12}$C, which would produce potential big bang signatures.

At the beginning of the r-process, nuclear statistical equilibrium assembles all the nuclei heavier than $^{12}$C in accordance with its prescription. However, the conditions that produce NSE are not thought to bring the nuclei lighter than $^{12}$C into NSE. $^{12}$C is the seed from which the nuclei formed in NSE are created, and which subsequently serve as the r-process seeds. One of the ways to circumvent the mass 5 and 8 gaps is via the $^{8}\mathrm{Li}(\alpha,n)^{11}\mathrm{B}$ reaction.

This reaction has been measured several times previously, but always by putting a $^{8}$Li beam directly into a heavy ion counter filled with $^{4}$He gas and using the tracks to determine which of the $^{8}$Li ions interacted with $^{4}$He nuclei to produce $^{11}$B. This is probably a fairly reliable technique at energies above 2 MeV, but becomes difficult to use at lower energies, especially those below 1 MeV that are of interest to big bang nucleosynthesis and the r-process.

Thus we hope to use the $^{8}$Li beam at TRIUMF to study this reaction, but to use quite a different technique to measure the cross section. We would use neutron time-of-flight measurements, which should completely circumvent the detection difficulties of the previous experiments. A 1 m$^{2}$ neutron wall from RIKEN will be brought to TRIUMF for the experiment. A special $^{4}$He gas cell will be built to produce the interactions. Prior to the experiment, a $^{13}$C beam will be used to produce the neutrons that will be used to calibrate the neutron wall detectors.

## Experiment 823
## Pure Fermi decay in medium mass nuclei
*(G.C. Ball, TRIUMF)*

Precise measurements of the intensities for superallowed Fermi $0^+ \rightarrow 0^+$ $\beta$ decays have provided a demanding test of the CVC hypothesis at the level of $3 \times 10^{-4}$ and also led to a result in disagreement with unitarity (at the 98% confidence level) for the CKM matrix [Towner and Hardy, Proc. WEIN '98 (World Scientific, Singapore, 1999) p.318]. Since this would have profound implications for the minimal standard model it is essential to address possible "trivial" explanations for this apparent non-unitarity, such as uncertainties in the theoretical isospin symmetry-breaking correction. Uncertainties in the calculated Coulomb corrections can be studied by extending the precision $\beta$-decay measurements to heavier (A $\geq$ 62, $T_z = 0$) odd-odd nuclei where these corrections are predicted to be much larger [Ormand and Brown, Phys. Rev. **C52**, 2455 (1995)]. The primary goal of the Expt. 823 experimental program is to measure the half-lives and branching ratios for the superallowed $\beta$-decay of these radioactive nuclei produced at ISAC.

### Precision measurement of the lifetime of $^{74}$Rb

A precision measurement of the lifetime of $^{74}$Rb was carried out at ISAC in 1999. Details of this experiment and preliminary results were reported previously [see 1999 Annual Report]. A proton beam of 10 $\mu$A was used to bombard a Nb foil target to produce $\sim$4000 $^{74}$Rb ions s$^{-1}$. A total of 38 runs, each consisting of $\sim 4 \times 10^5$ events, were carried out. The statistical error in the half-life of $^{74}$Rb obtained by fitting each decay curve was $\sim$0.14 ms. No evidence of any systematic error was observed, as illustrated by the fit to the full data set shown in Fig. 47 which gives a normalized $\chi^2 = 1.06$. The weighted average of all measurements was 64.768 $\pm$ 0.026 ms; the error quoted is statistical only. A complete analysis of the systematic errors together with an independent analysis of the same data set with different prescreening criteria led to a value of 64.761 $\pm$ 0.031 ms, which includes a systematic error of 0.015 ms added in quadrature. This is the first precision measurement of any of the key decay properties for an odd-odd $N = Z$ nucleus with A $>$ 54. A paper describing this measurement has been accepted for publication in Phys. Rev. Lett.

### Search for $\beta$-delayed $\gamma$ emission in the decay of $^{74}$Rb

An experiment to search for allowed transitions in the $\beta$-decay of $^{74}$Rb to excited $(0,1)^+$ states in $^{74}$Kr was carried out using a technique similar to that used

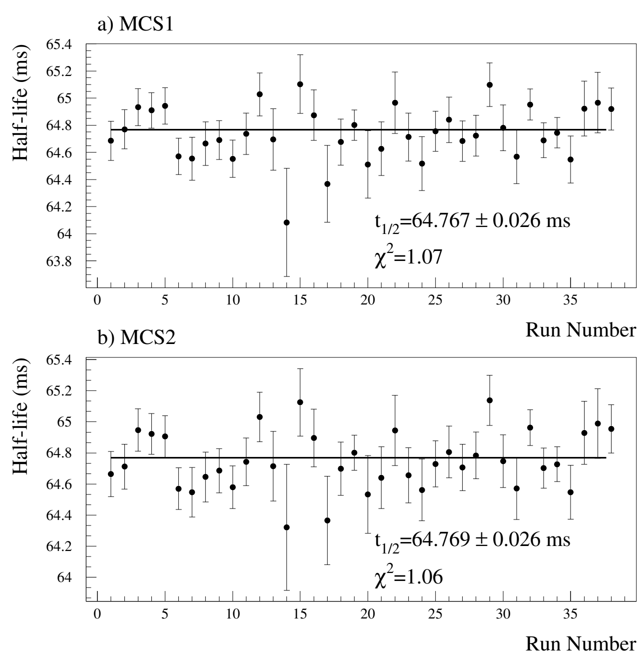


Fig. 47. Half-life results for $^{74}$Rb obtained simultaneously with two independent multi-channel scalar modules.

in previous measurements [Hagberg *et al.*, Nucl. Phys. **A571**, 555 (1994)]. The fast tape transport system described previously [1999 Annual Report] was used to collect and move the $^{74}$Rb samples out of the vacuum chamber and position them between two thin plastic scintillator paddles each backed by large (~80%) HPGe detectors mounted colinearly. The cycle time was reduced from that used in the lifetime measurements by shortening the counting time to 0.5 s. The background in the HPGe detectors resulting from positrons was reduced substantially (see Fig. 48) by accepting only those $\beta$-$\gamma$ coincidence events in which a positron was detected in the scintillator paddle located on the opposite side of the tape to the HPGe detector. The $\beta$-$\gamma$ coincidence events were time stamped and recorded event by event. The signals from each paddle were also multiscaled to obtain the $\beta$ singles rate. A total of ~15 M positrons were detected, resulting in ~1 M $\beta$-$\gamma$ coincidence events. The efficiencies of the HPGe detectors were measured using standard sources. In addition, the $\beta$-$\gamma$ coincidence efficiencies were determined by measuring the $\beta$-decay of $^{38}K_{gs}$ which has a strong branch (99.8%) to the first excited state of $^{38}$Ar that subsequently decays by the emission of a 2.168 MeV $\gamma$-ray. Finally, high statistics $^{74}$Ga decay data were obtained to better determine the isobaric contaminant background in the $^{74}$Rb $\gamma$-ray spectra.

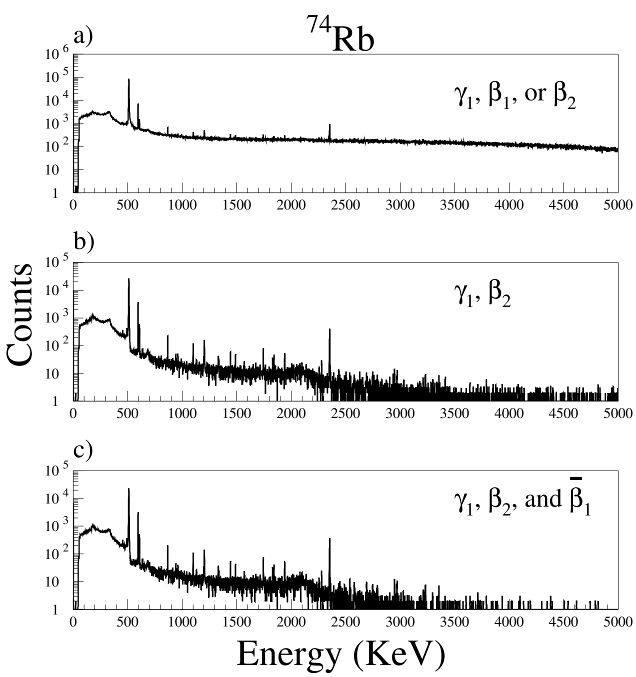


Fig. 48. $\gamma$-ray spectra obtained in the $\beta$-decay of $^{74}$Rb: a) in coincidence with positrons detected in either scintillator paddle, b) in coincidence with positrons detected in the paddle located on the opposite side of the tape from the HPGe detector and c) same as in b) with the additional condition that no positron signal was observed in the scintillator paddle positioned directly in front of the HPGe detector.

The analysis of these data is in progress. Weak Gamow-Teller/Fermi decays to one or more high-lying levels in $^{74}$Kr were observed by their depopulation through the known first excited $2^+$ level at 456 keV. Preliminary results indicate that the superallowed branch is the dominant transition (>99%), similar to those observed previously for odd-odd $T_z = 0$ superallowed decays. The limits that can be set for possible high-energy (~2–5 MeV) $\gamma$-rays resulting from the $\beta$ decay of $^{74}$Rb to higher-lying levels in $^{74}$Kr are $\lesssim$0.1%.

**Search for the non-analogue transition in the $\beta$ decay of $^{74}$Rb to the $0_2^+$ state in $^{74}$Kr**

The determination of the transition strengths for non-analogue $0^+ \rightarrow 0^+$ decays provides a critical test of the model predictions for the isospin mixing component of the Coulomb correction for superallowed $\beta$ decays. Recently, in-beam experiments [Chandler *et al.*, Phys. Rev. **C56**, R2924 (1997); Becker *et al.*, Eur. Phys. J. **A4**, 103 (1999)] have revealed the existence of a low-lying, isomeric $0_2^+$ level in $^{74}$Kr at 508 keV which decays primarily by an electric monopole transition to the ground state of $^{74}$Kr. A preliminary experiment to search for the $\beta$ decay of $^{74}$Rb to this excited $0_2^+$ level was carried out in May-June at a new target station, GP2, provided by TRIUMF. Most of the experimental hardware was provided by new Expt. 823 collaborators from LSU. In this measurement the $^{74}$Rb atoms were implanted into a 6 mm wide mylar tape of a moving tape-transport system that operated in vacuum. The collection point was viewed by two large plastic scintillation counters (one thin $\Delta$E counter and one thick E counter) to detect positrons, three $LN_2$-cooled Si(Li) diodes for the detection of conversion electrons and an (~80%) HPGe detector for $\gamma$-rays. Both Si(Li)-plastic and Ge-plastic coincidence data were recorded. The tape was moved every 5 s to reduce the background from the decay of $^{74}$Kr and $^{74}$Ga. The $\beta$ singles events were scaled and recorded for each 5 s counting cycle. A weak transition was observed in the Si(Li) spectra at 495 keV corresponding to the decay of the 508 keV level in $^{74}$Kr. From an analysis of these data it should be possible to measure the lifetime for the decay of this level. The efficiencies of the Si(Li) detectors were determined using a $^{207}$Bi source. Unfortunately, from these data, it will not be possible to obtain a precise measurement of the transition strength for this decay branch since a small (<5%) fraction of the radioactive beam was not deposited on the tape, resulting in a build up of long-lived $^{74}$Ga/$^{74}$Kr activity which made it more difficult to determine the $\beta$ singles rate coming from the decay of $^{74}$Rb. A new 13 mm wide tape transport system is being designed to eliminate this problem. In addition, in a test run it has been demonstrated that if the mass separator is operated in the high resolution mode, most of the contaminant $^{74}$Ga can be eliminated. This results in a factor of two loss in $^{74}$Rb beam intensity; however, if the proton beam current on the Nb target is increased from 10 to 20 $\mu$A then it has been shown that the yield of $^{74}$Rb increases by a factor of four.

The coincident $\gamma$-ray spectra obtained in this experiment contained a much higher $^{74}$Ga background component than those measured with the in-air tape-transport system. However, by setting a high energy gate on the coincident $\beta$ energy spectrum observed with the thick plastic scintillation detector, it was possible to observe the decay of the 456 keV level in $^{74}$Kr. These $\gamma$-ray spectra would also be greatly improved if we could eliminate the $^{74}$Ga isobaric contaminant. Furthermore, since a large fraction (>80%) of the available radioactive atoms decay in front of the detectors it should be possible to reduce the lower limits on possible high-energy (>2 MeV) $\gamma$-rays resulting from the $\beta$-decay of $^{74}$Rb to higher-lying levels in $^{74}$Kr.

### High-precision lifetime measurement for $^{38m}$K

A measurement of the half-life of $^{38m}$K, one of the nine well-known superallowed $\beta$-emitters, provides an important test of the experimental apparatus. As reported previously [1999 Annual Report], a high-precision lifetime measurement for $^{38m}$K is complicated by the long-lived isobaric contaminant $^{38}K_{gs}$ which is produced at ~100 times the yield of $^{38m}$K. A preliminary measurement of the half-life of $^{38m}$K was carried out in May, 1999. A more complete data set was obtained in August, 2000. To optimize the ratio for $^{38m}K$:$^{38}K_{gs}$, samples were collected for only ~0.3 s and the proton beam on the ISAC target was pulsed with a duty cycle of ~5–10%. As a result it was possible to increase the ratio for $^{38m}K$:$^{38}K_{gs}$ to ~60–80:1. A total of 31 runs, each consisting of ~4 M events, were obtained. The statistical error in the half-life of $^{38m}$K obtained by fitting each decay curve was ~0.6 ms. The weighted average of all measurements gave a preliminary value of 924.4 ± 0.1 ms (see Fig. 49). The errors quoted are statistical only and estimates of the systematic errors are in progress. The present result is in excellent agreement with the most precise value, 924.3 ± 0.3 ms, measured previously [Koslowsky *et al.*, Nucl. Phys. **A405**, 29, (1983)].

### Outlook

During the coming year the objectives are: 1) to complete the analysis of the precision lifetime measurements of $^{37}$K and $^{38m}$K and submit a paper for publication, 2) to complete the analysis of the precision branching ratio measurement for the decay of $^{74}$Rb,

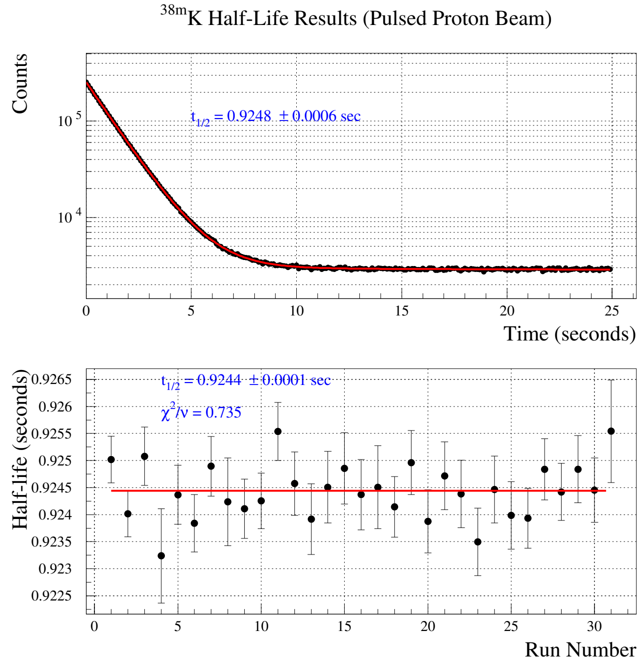


Fig. 49. $\beta$-decay half-life for $^{38m}$K obtained with the pulsed proton beam on the ISAC production target. The upper plot shows the fit to the data from one run. Below are shown the results from all runs and the (preliminary) mean values obtained.

3) to repeat the measurement of the branching ratio for the decay of $^{74}$Rb to the first excited $0^+$ state in $^{74}$Kr which decay by an E0 transition to the ground state, and 4) to measure the transition strength of the non-analogue $0^+ \rightarrow 0^+$ branch in $^{38m}$K.

## Experiment 826
## Studies of ultra-thin magnetic films with implanted isotopes
*(B. Turrell, UBC)*

The intention was to implant $^{91}$Rb first into iron. This decays to $^{91m}$Y and the hyperfine field of Y in Fe is accurately known. An NMRON run would then have been a good diagnostic test for the dilution refrigerator (DR) and the NMR-rf system.

We then planned to top-load a single crystal of terbium, obtained from Dr. W.D. Brewer, Free University of Berlin, implant $^{91}$Rb and again study the Y hyperfine field. The surface of the terbium crystal was polished down to 1 $\mu$m. Soldering terbium to copper is not easy, but a good join was made using indium as solder and *no* flux. In this procedure the terbium surface must be continually cleaned.

Unfortunately, neither of these experiments were carried out because the DR had developed a leak so that very low temperatures could not be attained.

The beam operators did produce a $^{91}$Rb beam. Analysis of the 2564 keV $\gamma$-ray in $^{91}$Sr from the decay of $^{91}$Rb showed an equilibrium count rate of 1.33

counts per second. Taking into account approximate values for the solid angle correction and the efficiency of the detector, we roughly estimate a yield for the $^{91}$Rb ion beam into the sample of $5 \times 10^4$ per second. This would have been sufficient to perform a nuclear orientation experiment. An NMRON experiment searching for the Y resonance in Tb would have been difficult, but not impossible, because of the relatively low count rate. The sweep in frequency would have been constrained to 4 MHz per hour so that 12 hours running would have only covered about 50 MHz. However, a lower limit on the resonant frequency could have been obtained from the $\gamma$-ray anisotropy.

## Experiments 838/864
## Double radiative decay of pionic atoms

*(T. Gorringe, P. Żołnierczuk, Kentucky)*

### Physics program with the RMC spectrometer

The RMC spectrometer is a large solid angle photon-pair spectrometer. It comprises a cylindrical Pb converter for $\gamma$-ray conversion, cylindrical drift and wire chambers for $e^+ - e^-$ tracking, and an axial magnetic field for momentum analysis. Fast triggering on photon events is accomplished through the hit patterns in concentric layers of plastic scintillators. For details see Wright *et al.*, Nucl. Instrum. Methods **A320**, 249 (1992).

During the past year our research program has involved the investigation of double radiative decay of pionic hydrogen (Expt. 838), double radiative decay of pionic deuterium (Expt. 864), and pion charge exchange at low energies (Expt. 869). Production runs on double radiative decay were conducted in April and commissioning runs for pion charge exchange were conducted in July and November.

### Experiment 838: Double radiative decay of the $\pi^-$H atom

The rare decay of pionic atoms by two-photon emission, $\pi^- A \rightarrow \gamma\gamma X$, was first considered by Ericson and Wilkin in Phys. Lett. **57B**, 345 (1975). They predicted the decay was dominated by annihilation of the stopped, real $\pi^-$ on a soft, virtual $\pi^+$ (i.e. $\pi\pi \rightarrow \gamma\gamma$). As discussed by Ericson and Wilkin and others, the $\pi\pi \rightarrow \gamma\gamma$ mechanism may provide sensitivity to both the electromagnetic properties of the charged pion and the pion field in the nuclear medium. Unfortunately the predicted branching ratio for double radiative decay is only $5 \times 10^{-5}$.

The goals of Expt. 838 were the first observation of the double radiative decay of the $\pi^-$H atom, the mapping-out of the photon angle and energy spectra, and the verification of the $\pi\pi \rightarrow \gamma\gamma$ mechanism. The major experimental difficulties are the very small branching ratio for double radiative decay and the very large two-photon background from pion charge exchange. Data were collected with a stopping $\pi^-$ beam and a liquid hydrogen target in December, 1998 and May, 1999 and yielded $\sim$1000 events from the double radiative decay of the pionic hydrogen atom. A typical event is shown in Fig. 50 and the two-photon opening angle distribution is shown in Fig. 51 (top). Our preliminary value for the branching ratio is $\mathrm{BR}_{[\pi^- p \rightarrow \gamma\gamma n]} = 3.8 \times 10^{-5}$. These results support the theoretical prediction for the dominance of the $\pi\pi \rightarrow \gamma\gamma$ mechanism.

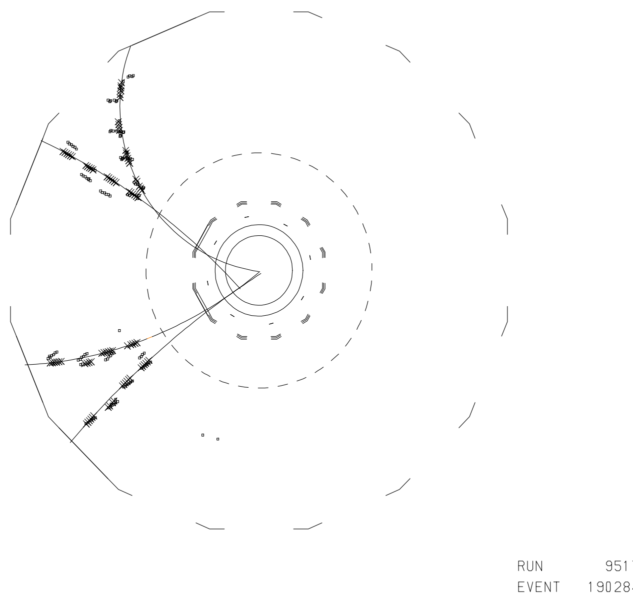


Fig. 50. A typical double radiative decay event from pionic hydrogen. It shows the two $e^+ - e^-$ pairs from photon conversion in the lead converter and characteristic pattern of trigger scintillator hits.

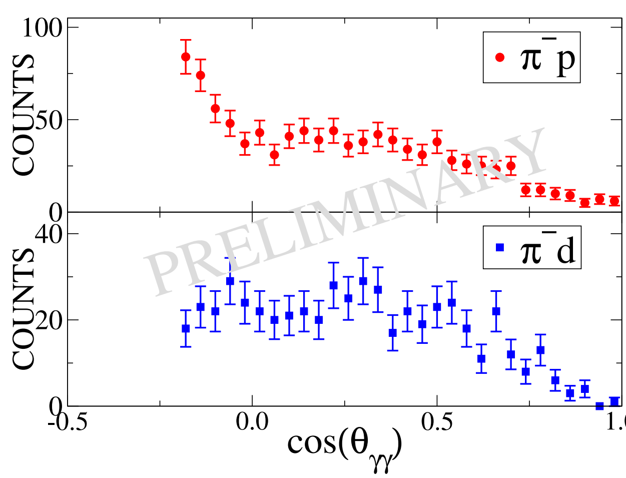


Fig. 51. The two-photon opening angle spectra for pionic hydrogen (top) and deuterium (bottom).

**Experiment 864: Double radiative decay of the $\pi^-$D atom**

Recently a group at JINR have made claims for the existence of a super-narrow $NN$-decoupled dibaryon – the $d_1^*(1920)$ [Khrykin *et al.*, $\pi N$ Newslett. **13**, 250 (1997)]. Their claims are based on the energy spectra of double bremsstrahlung events from proton-proton collisions. Subsequently, an assessment by Gerasimov has concluded that if the $d_1^*(1920)$ is observed in double bremsstrahlung from $p-p$ collisions, then the $d_1^*(1920)$ should be observed in double radiative decay of $\pi^-$D atoms.

The goals of Expt. 864 were twofold. Firstly, we aimed to employ the double radiative decay of pionic deuterium as a sensitive probe for the possible existence of the $d_1^*(1920)$ dibaryon. Secondly, together with our $\pi^-$H data and earlier $\pi^-$C data, we aimed at obtaining a first study of the $A$-dependence of the double radiative decay. Data were collected with a stopping $\pi^-$ beam and a liquid deuterium target in April and yielded ∼500 events from the double radiative decay of the pionic deuterium atom. Our preliminary result for the branching ratio is $\mathrm{BR}_{[\pi^-\mathrm{D}\to\gamma\gamma nn]} = 1.6\times10^{-5}$ and the two-photon opening angle distribution is shown in Fig. 51 (bottom). Our data show no evidence for production of the $d_1^*(1920)$ dibaryon.

**Experiment 863**
**Ground state magnetic moments of $^{75,77,79}$Ga (LTNO)**
*(P. Mantica, MSU)*

The focus of Expt. 863 is to study the evolution of the single-particle structure of medium-mass nuclides having $Z \geq 28$ toward the $N = 50$ shell closure. A well-known shape transition from spherical to moderate deformation ($\beta_2 \sim 0.2$) occurs in the neutron-rich $_{31}$Ga and $_{32}$Ge isotopes between $N = 40 - 42$. Since the ground state magnetic dipole moment can serve as a sensitive probe of the nuclear ground state wavefunction, the experimental determination of the magnetic moments of the heavy, odd-$A$ Ga isotopes can address the extent to which quadrupole deformation persists toward $N = 50$.

The ground state magnetic moments will be measured using the LTNO facility coupled to the low-energy channel at ISAC. The Ga isotopes of interest will be implanted into an iron foil maintained at ≈ 10 mK at the centre of the $^3$He/$^4$He dilution refrigerator. Nuclear magnetic resonance on oriented nuclei (NMR/ON) will be used to observe the destruction of the nuclear orientation and extract the ground state magnetic moment. Since Ga isotopes experience only a small hyperfine field in iron, the normal method of extracting orientation parameters from $\gamma$-ray angular

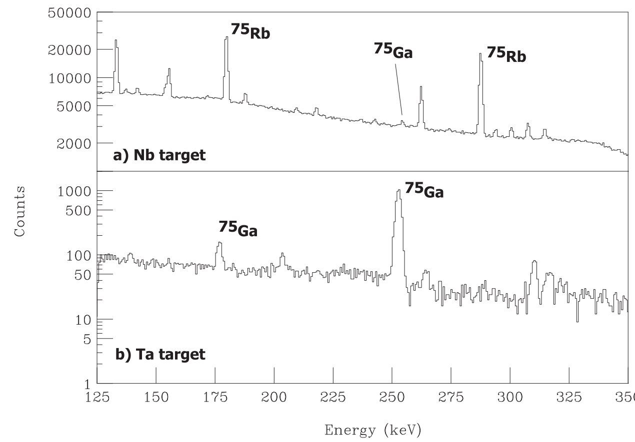


Fig. 52. $\gamma$-ray spectra at $A = 75$ for a) Nb and b) Ta ISAC production targets.

distributions will prove difficult. We have proposed, therefore, to measure the destruction of the angular distribution of $\beta$ particles emitted by the implanted Ga isotopes. The $\beta$ anisotropies are expected to show a larger effect due to reliance on the $B_1$ orientation parameter.

**Production of $^{75}$Ga**

Although the $\beta$-ray angular distributions are expected to be large for the heavy, odd-$A$ Ga isotopes, the main disadvantage in such a measurement is the continuous nature of the $\beta$-ray spectrum and difficulties with contamination from unwanted sources. For example, production of neutron-rich $^{75}$Ga from a surface ionization source may also result in significant production of neutron-deficient $^{75}$Rb. Since $^{75}$Rb and $^{75}$Ga have similar decay half-lives and $\beta$ endpoint energies, it would be difficult to differentiate the $\beta$ decays of these species.

Production tests for $^{75}$Ga have been performed at ISAC using production targets of Nb and Ta. Representative $\gamma$-ray spectra are shown in Fig. 52. Using the Nb target, the most significant yield at $A = 75$ is $^{75}$Rb. However, employing the more neutron-rich Ta production target strongly favours the production of $^{75}$Ga over $^{75}$Rb. The observed $^{75}$Ga/$^{75}$Rb ratio is adequate to complete the proposed $\beta$-NMR/ON measurements on $^{75}$Ga. Favourable $^{77}$Ga/$^{77}$Rb and $^{79}$Ga/$^{79}$Rb ratios have also been measured using the Ta production target at ISAC.

**Experiment 869**
**Pion charge exchange at low energies**
*(T. Gorringe, P. Żołnierczuk, Kentucky; M. Hasinoff, UBC)*

Isospin symmetry is central in understanding the structure and interactions of mesons and baryons. However, the symmetry is approximate; it being violated by the Coulomb interaction and the u,d-quark mass difference. The $\pi N$ system represents a fundamental arena for testing our understanding of isospin symmetry breaking. Interestingly, recent analyses of $\pi N$ elastic scattering and charge exchange data have suggested an unexpectedly large isospin violating effect. The key data in these analyses are the charge exchange data at $T_\pi \sim 50$ MeV and forward angles where destructive interference of $s$-/$p$-waves yields high sensitivity to possible effects of symmetry breaking.

The goal of Expt. 869 is a precision measurement of the pion charge exchange differential cross section at low energies and forward angles. The program requires a modification of the RMC detector to operate as a $\pi^0$ spectrometer. Such modifications include a new photon converter package, a new beam counter package, and a new trigger system. A new photon converter package is required to enable the determination of the $\pi^0$ momentum with the necessary accuracy. A new beam counter package is required to permit variable target positions, high accuracy $\pi^-$ counting, and minimal $\pi^-$ energy loss. The various modifications were successfully commissioned in two runs in July and November. Production running of Expt. 869 is scheduled for May, 2001.

## Experiment 875
## Muon scattering in low $Z$ materials for muon cooling studies

*(R. Edgecock, RAL; K. Nagamine, RIKEN)*

### Muon cooling

A vital requirement of the accelerator complex used to supply muons to a future neutrino factory or muon collider is the ability to cool the muons. In the case of the neutrino factory, the aim is a factor of 10 reduction in the normalized emittance in each transverse plane, while for a muon collider the requirement is a $10^6$ reduction in the 6-dimensional phase space. Due to the muon lifetime, such cooling needs to be fast and the currently preferred technique is ionization cooling [MUCOOL Collab., Fermilab Proposal P904 (1998)]. In the case of the transverse cooling required for a neutrino factory, this involves passing the muons through an absorber in which they lose both longitudinal and transverse momentum. The lost longitudinal momentum is then restored using rf cavities following the absorber.

As well as a cooling effect coming from the ionization energy loss, there is heating coming from multiple scattering and the final cooling achieved is a balance between these. Theory suggests this balance is most favourable for elements with low atomic number, in particular, liquid hydrogen. However, an extensive literature search has failed to find any measurements of the muon scattering distribution in light elements [Fernow, MUCOOL Note 123 (2000)]. The most relevant data found comes from the scattering of 2.7 MeV/c electrons on Al, Be and Li [Kulchitsky and Latyshev, Phys. Rev. **61**, 254 (1942); Andrievsky *et al.*, J. Phys. (USSR) **6**, 279 (1942)]. These data show a clear trend: as $Z$ decreases, the agreement with Moliere theory [Moliere, Z. Naturforschg. **3a**, 78 (1948); Scott, Rev. Mod. Phys. **35**, 231 (1963)] gets worse. If this trend continues to hydrogen, there will be two effects:

1. The level of cooling achieved would be less than expected.
2. Due to the increased scattering in the tails, the fraction of muons scattered out of the cooling channel could be much bigger than expected.

Due to the importance of this to ionization cooling, the MuScat experiment has been created to measure the scattering of muons of various momenta in a number of low atomic number materials, in particular liquid hydrogen. As well as checking these observations, MuScat will compare a range of muon scattering models with the data.

A four week test period was allocated to the MuScat experiment in the M11 beam line in June and July. The following sections will describe the experiment and show what was learnt about it during the run. The plans for a further run in 2001 will also be outlined.

### The MuScat experiment

As the aim of the experiment is to make a precise measurement of the multiple scattering of muons, the amount of material that the muons must pass through has to be kept to a minimum. For this reason, it is not possible to do any tracking before the target and a collimation system must be employed to reduce the beam dimensions so that the incoming particle position is known accurately enough. In addition, the measurement of the position of the scattered muon relies on the first tracking detector as all subsequent detectors will be affected by scattering in the first. Any additional detectors can only be used to aid in noise rejection and for checking systematics. To minimize scattering in air, as much of the experiment as possible must be mounted in vacuum. Finally, to eliminate particles other than muons, a good time-of-flight system is required.

The detector designed to satisfy these requirements and used in the M11 beam is shown in Fig. 53. The most upstream parts are a veto shield and veto scintillator to eliminate beam halo. These are followed by the first trigger counter, which also acts as the TOF start. This is built from two fingers of scintillator, each 1 mm thick, 28 mm long and 3 mm high. These overlap by 20 mm in length and 3 mm in height. The timing resolution is about 250 ps. The TOF stop comes from the

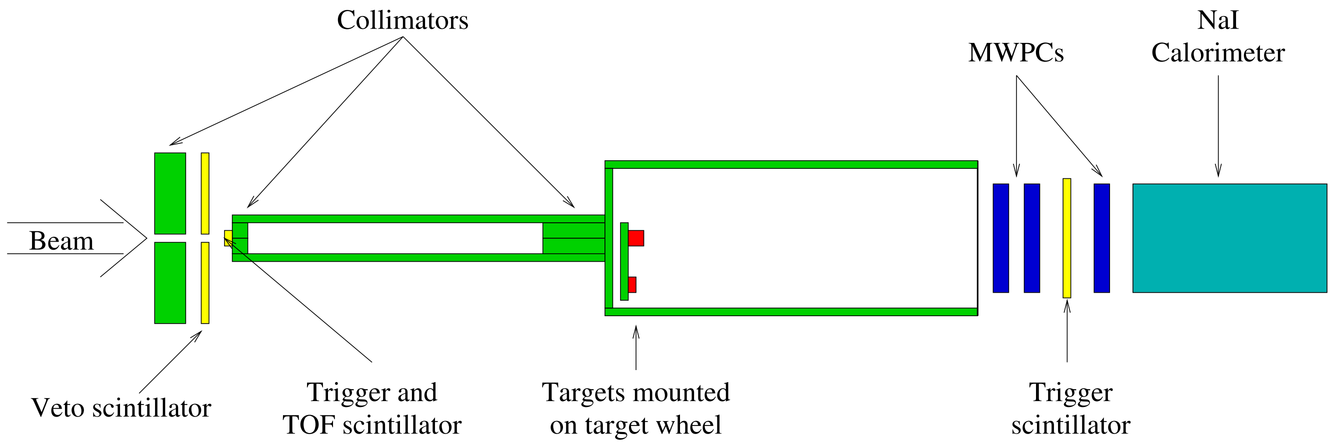


Fig. 53. Schematic longitudinal layout of the MuScat experiment.

following rf bucket of the cyclotron. This is almost a square-wave of length 1.9 ns, the smearing of the edges corresponding to a resolution of about 500 ps.

This trigger scintillator is followed by a 1 m long vacuum tube containing the collimation system. This consists of a 40 mm thick lead block at the front and a 160 mm thick lead block at the back, plus 4 intermediate blocks each 10 mm thick, which are not shown in the figure. The first block has a slit 20 mm long by 2 mm high cut in it, while the slot in the second block is tapered to prevent large angle scatters off the internal face. With this arrangement, the scattering distribution is measured vertically, in the narrow direction of the slot. The second dimension is longer to increase the particle intensity.

The vacuum tube is connected to the main vacuum vessel, which contains the targets. These are:

- Liquid hydrogen, 100 mm and 150 mm thick
- Lithium, 10 mm and 2.5 mm thick
- Beryllium, 2 mm and 0.5 mm thick
- Carbon, 2.5 mm thick
- Aluminum, 1 mm thick
- $CH_2$, 2 mm thick
- Iron, 0.15 mm and 2 mm thick

The "thick" iron sample is used simply to blow the beam up to give a better coverage of the detectors and improve the measurement of the efficiency. The liquid hydrogen targets were not used during the 2000 run, but are being designed for the second run in 2001. In addition, the possibility of including a LiH target, which is the best candidate absorber for ionization cooling after hydrogen, is being investigated.

The solid targets are mounted on a target wheel that can be controlled from outside the vacuum so it is unnecessary to break this each time a target is changed. The wheel has 10 slots, the last of which has no target mounted and is used to measure the intrinsic properties of the beam. These are monitored on a regular basis.

The tracking detectors used are delay-line chambers. These are multi-wire proportional chambers with two 2 cathode planes and 1 anode plane. Each chamber gives 2-dimensional readout, but with better resolution from the cathode plane perpendicular to the anode plane, ~0.6 mm compared to 1–2 mm. Rather than each wire being read out, the number of electronics channels required is reduced by recording only two signals from each plane. These are time values, giving the position along the delay-line from which the signal originated. As shown in Fig. 53, three of these chambers are used, each 300 mm by 300 mm in size. The most important of these is the first, which is oriented such that the dimension with the better resolution is vertical. It is approximately 1 m from the target wheel. Between the second and third chambers is the second trigger scintillator.

The final part of the detector is MINA, a NaI calorimeter of 360 mm diameter and 360 mm depth [Waltham *et al.*, Nucl. Inst. Meth. **A256**, 91 (1987)]. It has a measured energy resolution (fwhm) of 5.2% at 90 MeV with an energy dependence of $E^{-0.55}$. It is used for both a muon energy measurement and additional pion/muon separation.

#### Performance

As already mentioned, a period of 4 weeks was allocated to the experiment in the M11 beam line, including 1 week of setting up. Three beam momenta were used: 130, 150 and 180 MeV/c. However, of these, 180 MeV/c is the most interesting and all the results shown will come from data at this momentum.

##### Delay-line chambers

During the first 8–10 days of data-taking, a steady and spatially non-uniform drop in the efficiency of two of the delay-line chambers was noted. Examination of one chamber showed that this was due to wrinkling of the cathode plane and it was thought that this resulted from too high a concentration of the methylal vapour in the argon-isobutane gas mixture. Ultimately, the two most upstream chambers were replaced and the temperature of the methylal bath was reduced to lower the vapour pressure. The measured efficiency of the most upstream chamber (PC2) from a subset of the runs taken after the change is shown in Fig. 54, as a function of vertical and horizontal position. This still indicates a non-uniform efficiency and it has been concluded that these data cannot be used for precise measurements of the muon scattering distribution. Nevertheless, they are proving very useful for checking how the detector works and there have been significant modifications as a result. These studies and the changes implied for the next running period are discussed in the following sections.

In light of the problems with the delay-line chambers, it has been decided to build new tracking chambers for the next run. They will be constructed from crossed planes of scintillating fibres. These will provide a high and uniform efficiency, an improved position resolution of about 200 $\mu$m, and a time resolution of 150 ps. In addition, it will be possible to mount the chambers inside the vacuum and eliminate any material between the target and the first detector. A new vacuum vessel is being designed for this purpose.

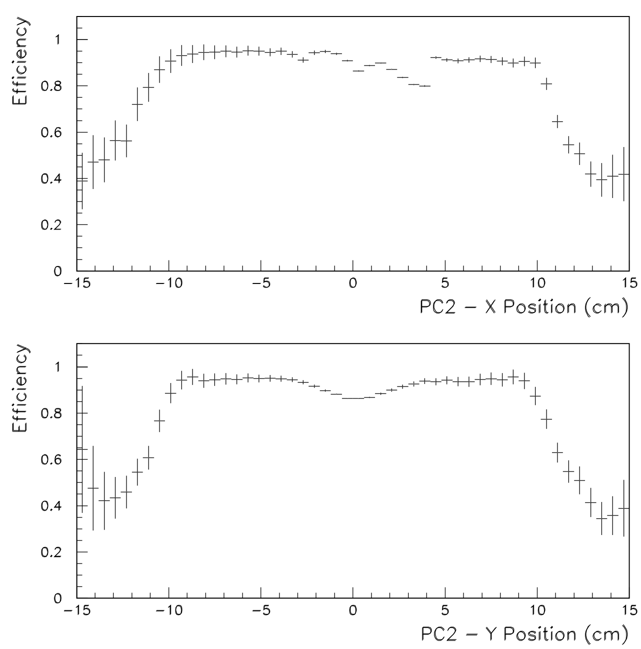


Fig. 54. Efficiency of the most forward delay-line chamber as a function of X (horizontal position) and Y (vertical position).

**Event rate**

This was important to measure as the fineness of the collimation system could potentially have reduced the muon event rate to an impractical level. The measured rates of events to disk are listed in Table XII. Note that at higher momentum, these are strongly affected by deadtime. The total trigger rate is dominated by pions, so the muon rate is estimated using the muon fraction in the beam determined from the time-of-flight plot (see Fig. 55). As $10^6$ muons are required per measurement, it typically takes 10 hours for each of these in M11.

Table XII. Measured event rates and the fraction of muons in the beam at the three beam momenta used in 2000.

| $p$ (MeV/c) | Total rate (Hz) | $\mu$/total | $\mu$ rate (Hz) |
|---|---|---|---|
| 130 | 210 | 0.10 | 21 |
| 150 | 270 | 0.09 | 24 |
| 180 | 550 | 0.06 | 33 |

**Time-of-flight resolution**

Figure 55 shows the difference in time between the arrival of a particle in the TOF scintillator and the next rf beam pulse, in TDC counts, at 180 MeV/c. Note that as the difference is taken with respect to the next beam pulse, the particle velocity increases along the $x$ axis. The time separation between the pions and muons is 4.9 ns and between muons and electrons is 7.5 ns.

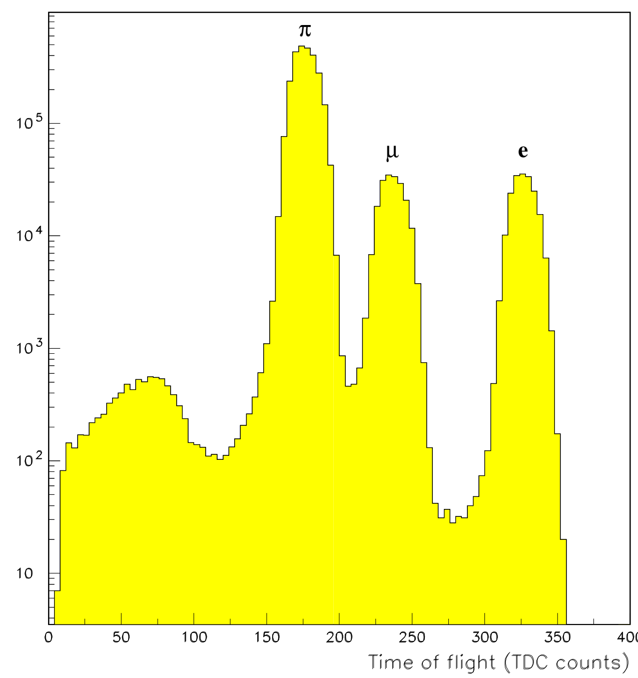


Fig. 55. Measured time of flight at 180 MeV/c using the MuScat detector in the M11 beam at TRIUMF. The $\pi$, $\mu$ and $e$ peaks are indicated. The broad peak at low velocity comes from protons.

There is a clear separation between the muons and the other particles, allowing a muon signal to be extracted with a negligible background.

#### Collimation system

Selecting muons using the TOF distribution shown in Fig. 55, the vertical projection of the distribution of these muons in the most upstream delay-line chamber with a 9.5 mm Li target and no target are compared in Fig. 56. To extract the scattering distribution from these, a rigorous unfolding procedure using the maximum entropy technique [see Maximum Entropy and Bayesian Methods, Skilling, ed. (Kluwer Academic, 1989)] is being developed and will be used to determine whether or not the tails in the no target case are being reduced sufficiently by the collimation system. However, simpler techniques are already indicating that this may not be the case. As a result, simulation studies are under way to determine where the tails originate and how they can be further reduced using both additional collimators and veto scintillators.

#### Conclusion

The MuScat experiment has been designed and built to make a precise measurement of the scattering distribution of muons of momentum in the range 150–180 MeV/c in a number of materials of low atomic number. The performance of the experiment was tested in a run in the M11 beam in the summer. Although largely successful, much has been learnt from this and a number of alterations will be made for a second run in 2001. The main change will be a new set of tracking detectors to replace the delay-line chambers used in 2000.

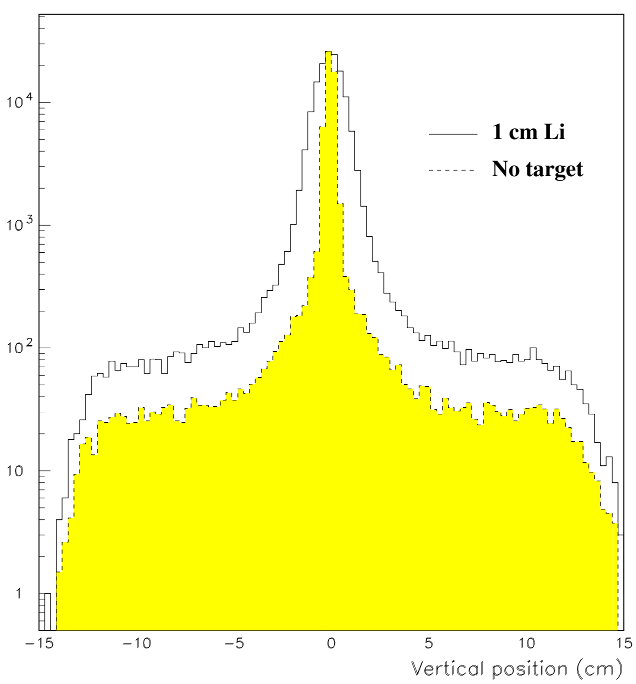


Fig. 56. Vertical projection of the muon distribution in the first delay-line chamber with no target (shown shaded) and with 10 mm of Li. The muons are selected using time of flight.

### Experiment 880
### Ortho-para effect of muon catalyzed fusion in solid deuterium

*(K. Ishida, K. Nagamine, RIKEN/KEK)*

The experiment was aimed at measuring the dependence of the rate of muon catalyzed fusion in the $D_2$ system ($dd$-$\mu$CF) on the ortho-para state of deuterium molecules. In the $dd$-$\mu$CF process, the resonant formation of $dd\mu$, $d\mu + D_2 \to [(dd\mu)dee]$ is one of the most important processes determining the overall efficiency of producing fusion neutrons. Since this process requires an energy matching between the initial state and the final state, the rate is very sensitive to the states of $d\mu$ (hyperfine states $F = 3/2$ or $1/2$, kinetic energy, etc.) and $D_2$ (vibrational and rotational molecular states, kinetic energy, etc.). Although the system had been experimentally investigated by changing various parameters such as the temperature and the density, full understanding was not yet achieved. In order to obtain further understanding of this process, we started to investigate the effect of another parameter, namely the ortho-para state of the $D_2$ molecule.

Especially, the measurement would be used to solve the puzzling “solid-state” effect in $dd$-$\mu$CF. It had been expected by theoretical calculations that the $dd\mu$ molecular formation rate decreases rapidly by decreasing the deuterium target temperature below 20 K, but it was actually found by measurements that the rate stays nearly constant in the solid even down to 3 K. In some of the proposed explanations the para deuterium contributes an essential role, so an experiment with a controlled ortho-para ratio would be a critical test on the contribution of para $D_2$.

The measurement was performed at the M9B channel in June. The set-up consisted of a 3.5 K solid deuterium target system with cryostat, a deuterium gas handling system with an ortho-para converter and an ortho-para analyzer, and the detection system for incoming muons, muonic X-rays, fusion protons and $\mu \to e$ decay electrons.

To control the ortho-para ratio of the deuterium gas, we passed the normal deuterium gas (67% ortho and 33% para) through an ortho-para conversion chamber which contained a catalyst ($Cr_2O_2$ + $Al_2O_2$ powder) maintained at low temperature (typically 12.5 K). This produced an ortho-rich deuterium (99.7% ortho and 0.3% para). The deuterium gas was then solidified on a thin silver foil maintained at 3.5 K to make a solid $D_2$ target of 40 mm in diameter and 0.3 mm in thickness. The measurement was carried out for three different target conditions, namely for 67%-ortho "normal" $D_2$, for 99.7%-"ortho" $D_2$, and for silver substrate foil only. The target was irradiated by the negative muon beam and the muonic X-rays as well as protons from *dd*-fusion were detected. The muonic X-rays gave us the number of stopped muons in deuterium as well as being used to determine the upper limit of the impurity level in the deuterium target. For the *dd*-fusion proton detection we used silicon surface barrier (SSB) detectors in pairs, so that the "$\Delta E$ vs. $E$" particle identification method was applied. This enabled us to clearly separate fusion protons from other particles such as muons and deuterons. The fusion proton emission time spectrum after muon stopping was analyzed to extract various parameters such as the effective $dd\mu$ formation rate from the $d\mu(F{=}3/2)$ state, $\tilde{\lambda}_{\frac{3}{2}}$, and the hyperfine transition rate from the $d\mu(F{=}3/2)$ to $d\mu(F{=}1/2)$ state, $\tilde{\lambda}_{\frac{3}{2}\frac{1}{2}}$.

In Table XIII we present a preliminary result of the analysis about these rates for normal $D_2$ and ortho $D_2$.

1. The effective $dd\mu$ formation rate as well as hyperfine transition rate is decreased by decreasing the para concentration.
2. Even so, we still see a fast $dd\mu$ formation rate in the ortho $D_2$ in which the para-$D_2$ concentration is very small. This result strongly rejects some of the models proposed to explain the "solid-state" effect, such as those assuming that $d\mu$ is heated by collision with para-$D_2$.
3. The relative effect of the ortho-para conversion seen in the hyperfine transition rate is roughly half of that in the effective $dd\mu$ formation rate. From this, the hyperfine transition via back-decay from the $dd\mu$-molecule was estimated to contribute nearly half of the total hyperfine transition rate (the other half is the direct spin exchange process which is not dependent on the $D_2$ molecular state). A detailed analysis is in progress.

Table XIII. Obtained values (preliminary) of the effective $dd\mu$ formation rate $\tilde{\lambda}_{\frac{3}{2}}$ and the hyperfine transition rate $\tilde{\lambda}_{\frac{3}{2}\frac{1}{2}}$ in normal $D_2$ and ortho $D_2$, and the relative effect due to ortho-para conversion.

| | Normal $D_2$ | Ortho $D_2$ | Effect |
|---|---|---|---|
| $\tilde{\lambda}_{\frac{3}{2}}$ | 2.299(69) | 1.611(40) | –30(4)% |
| $\tilde{\lambda}_{\frac{3}{2}\frac{1}{2}}$ | 40.3(14) | 34.4(9) | –15(4)% |